Journal of Experimental & Clinical Cancer Research

RESEARCH

Open Access

Essential role of PLD2 in hypoxia-induced stemness and therapy resistance in ovarian tumors

Sandra Muñoz-Galván[1,2*], Eva M. Verdugo-Sivianes[1,2], José M. Santos-Pereira[3], Purificación Estevez-García[1,2] and Amancio Carnero[1,2*]

Abstract

Background Hypoxia in solid tumors is an important source of chemoresistance that can determine poor patient prognosis. Such chemoresistance relies on the presence of cancer stem cells (CSCs), and hypoxia promotes their generation through transcriptional activation by HIF transcription factors.

Methods We used ovarian cancer (OC) cell lines, xenograft models, OC patient samples, transcriptional databases, induced pluripotent stem cells (iPSCs) and Assay for Transposase-Accessible Chromatin using sequencing (ATAC-seq).

Results Here, we show that hypoxia induces CSC formation and chemoresistance in ovarian cancer through transcriptional activation of the *PLD2* gene. Mechanistically, HIF-1α activates *PLD2* transcription through hypoxia response elements, and both hypoxia and *PLD2* overexpression lead to increased accessibility around stemness genes, detected by ATAC-seq, at sites bound by AP-1 transcription factors. This in turn provokes a rewiring of stemness genes, including the overexpression of *SOX2*, *SOX9* or *NOTCH1*. *PLD2* overexpression also leads to decreased patient survival, enhanced tumor growth and CSC formation, and increased iPSCs reprograming, confirming its role in dedifferentiation to a stem-like phenotype. Importantly, hypoxia-induced stemness is dependent on *PLD2* expression, demonstrating that PLD2 is a major determinant of de-differentiation of ovarian cancer cells to stem-like cells in hypoxic conditions. Finally, we demonstrate that high *PLD2* expression increases chemoresistance to cisplatin and carboplatin treatments, both in vitro and in vivo, while its pharmacological inhibition restores sensitivity.

Conclusions Altogether, our work highlights the importance of the HIF-1α-PLD2 axis for CSC generation and chemoresistance in OC and proposes an alternative treatment for patients with high *PLD2* expression.

Keywords Ovarian cancer, Hypoxia, Phospholipase D, Therapy resistance, Stemness

*Correspondence:
Sandra Muñoz-Galván
smunoz-ibis@us.es
Amancio Carnero
acarnero-ibis@us.es
[1]Instituto de Biomedicina de Sevilla, IBIS, Hospital Universitario Virgen del Rocío, Universidad de Sevilla, Consejo Superior de Investigaciones Científicas, Avda. Manuel Siurot s/n 41013, Seville, Spain
[2]CIBERONC, Instituto de Salud Carlos III, Madrid, Spain
[3]Centro Andaluz de Biología del Desarrollo (CABD), Consejo Superior de Investigaciones Científicas, Universidad Pablo de Olavide, Seville 41013, Spain

Background

Hypoxia is a common feature of the tumor microenvironment in solid tumors [1]. Hypoxia is generated by insufficient oxygen diffusion towards parts of the tumor that are not irrigated, although the highly irregular tumor microvasculature may also generate hypoxic regions. Cancer cells under hypoxic conditions undergo a series of transcriptional changes that are induced by hypoxia-inducible factors (HIF), HIF-1, -2 and −3, with HIF-1 being the best known [2–4]. HIFs are heterodimeric transcription factors containing bHLH-PAS domains and consist of an α subunit regulated by oxygen levels and a constitutively expressed β subunit (also called ARNT) [5]. The HIFa-ARNT dimers bind DNA at specific sequences known as hypoxia-response elements (HREs) to promote target gene expression [6]. In normoxia, HIF-α subunits are hydroxylated at specific proline and asparagine residues by prolyl hydroxylase 2 (PHD2) and are recognized and targeted for degradation by the von Hippel–Lindau (VHL) tumor suppressor. However, hypoxia leads to the inhibition of such hydroxylation and subsequent HIF-α accumulation, heterodimerization with ARNT and transcriptional activation of target genes [7]. The multiple effects of hypoxia on the biology of tumors include preventing apoptosis and promoting proliferation and autophagy, inducing metabolic alterations, and promoting angiogenesis, the epithelial-to-mesenchymal (EMT) transition, invasion and metastasis [8, 9]. Indeed, HIF-1α is overexpressed in multiple tumor types and is associated with a poor prognosis in patients and therapy resistance [10–17].

Ovarian cancer (OC) is the most lethal gynecological malignancy [18] mainly due to its nonspecific clinical manifestations, which lead to a late diagnosis and high chemoresistance [19]. Similar to other solid tumors, hypoxia is a key modulator of the tumor microenvironment in OC, affecting not only the primary tumor but also the ascitic fluid, which is the main route of spread of these malignancies and shows low oxygen levels [12, 20]. Therefore, ovarian tumors are highly hypoxia-dependent and this dependency influence the response to treatment. A major cause of chemoresistance is the persistence of a cancer cell subpopulation known as cancer stem cells (CSCs) or tumor-initiating cells. CSCs are able to recapitulate a new tumor since they possess self-renewal and pluripotency properties similar to those of normal stem cells [21, 22]. CSCs are resistant to common antitumor therapies, which may indeed cause their enrichment, leading to chemoresistance and relapse [23, 24]. Several studies indicate that HIF-1 is required for maintaining CSCs and that its activation in hypoxia leads to the increased expression of stem marker genes in multiple cancer types [25, 26]. Therefore, hypoxia may promote the generation of CSCs leading to chemoresistance through HIF factors, but our knowledge of HIF targets that may be responsible for CSC activity is limited.

We previously showed that the *PLD2* gene, encoding phospholipase D2, is overexpressed in colorectal cancer and induces stemness in cancer cells through communication with the tumor microenvironment [27]. Here we find that *PLD2* is also overexpressed in ovarian cancer patients, being associated with poor patient survival. We explore a possible connection of *PLD2* with hypoxia in OC and demonstrate that *PLD2* expression in OC cells is stimulated by hypoxia and that HIF-1α promotes *PLD2* transcription through HREs at its promoter and an intronic enhancer. This leads to increased chromatin accessibility around stemness genes, which are in turn overexpressed provoking an enhancement of tumor growth and formation of CSC-like tumorspheres. This is corroborated by induced pluripotent stem cell (iPSC) reprogramming experiments that confirm the role of hypoxia and PLD2 in dedifferentiation of OC cells to stem-like cells. Importantly, the increase in CSC-like features induced by hypoxia relies on *PLD2* expression, indicating that the hypoxia-PLD2 axis is a major contributor to tumor stemness. We confirm these findings in transcriptional databases of OC patients, where high *PLD2* expression is associated with a transcriptional rewiring of genes involved in the hypoxia response and in the maintenance of stem cells. Finally, we show that *PLD2* overexpression causes resistance to platinum-based compounds and propose a new therapy based on pharmacological inhibition of phospholipases D to suppress such chemoresistance.

Methods

Cell culture

Cells were cultured according to the manufacturer's recommended procedures in McCoy (ES-2 line) or RPMI (SKOV3 and OVCAR8 lines) and incubated at 37 °C in 5% CO_2 in a humidified atmosphere.

Gene transfer

The gene transfer was performed as previously described [28]. The PLD2 overexpression plasmid was described in [27]. The shRNA against *PLD2* was provided by Origene.

Proliferation assay

The proliferation assay was performed as previously described [28].

Cytotoxic assay

ES-2, SKOV3 or OVCAR8 cells were seeded and then treated with platinum drugs and/or the PLD inhibitor 5-Fluoro-2-indolyl des-chlorohalopemide (FIPI) at 300nM concentration 24 h later. After 96 h, cells were stained with 0.5% crystal violet. Then, the crystal

violet was solubilized in 20% acetic acid and quantified at 595 nm absorbance to measure the cell viability.

Maintenance of mouse colonies

All experiments involving animals received expressed approval from the IBIS/HUVR Ethical Committee for the Care and Health of Animals. The mice were maintained in the IBIS animal facility according to the facility guidelines, which are based on the Real Decreto 53/2013 and were sacrificed by CO_2 inhalation either using a planned procedure or as a human endpoint when the animals showed significant signs of illness.

Colony formation assay and clonal heterogeneity analysis

This analysis was performed as previously described in [28]. Briefly, in total, 10^3 cells were seeded onto 10 cm plates, and every condition was evaluated in triplicate. The medium was replaced every 3 days for 12 days, and the colonies were fixed, stained and counted. The values are expressed as the number of observed colonies among the 10^3 seeded cells. To analyze the clonal heterogeneity, 10^2 random colonies were classified in triplicate as having the following phenotypes: holoclone, meroclone and paraclone [29], which are considered stem cells, transit-amplifying cells and differentiated cells, respectively [30].

Sphere-forming assay

In total, 2×10^3 cells were resuspended in 1 ml of complete MammoCultTM Basal Medium (Stemcell Tech) and seeded in ultralow attachment plates. The cultures were imaged, the tumorspheres were counted, and their diameters were quantified using CellSenseDimension software on Days 2, 3 and 4.

Western blot analyses and immunofluorescence were performed according to standard procedures. Information of antibodies and dilutions is shown in Supplementary Table S1, Additional File 1.

RT–qPCR

The total RNA was isolated using an RNeasy kit (Qiagen), and cDNA was generated from 1 µg of RNA with MultiScribe Reverse Transcriptase (Applied Biosystems). qPCR was performed using a TaqMan Assay (Applied Biosystems) with probes. The relative mRNA expression was calculated as $2^{-\Delta Ct}$ relative to the *ACTB* gene. Information of probes is shown in Supplementary Table S1, Additional File 1.

Fluorescence-activated cell sorting

For FACS staining, live cells were incubated with antibodies for 30 min at dilutions specified in the manufacturer's protocols.

iPSCs protocol

Briefly, mouse embryonic fibroblasts (MEFs) were infected with 4 different retroviral vectors encoding the Yamanaka factors (pMXs-Oct3/4, pMXs-Sox2, pMXs-Klf4, and pMXs-cMyc), an additional lentiviral vector that expresses GFP in cells where the Nanog promoter/enhancer is active (mNanog-pGreenZeo), and the corresponding plasmid overexpressing PLD2, carrying shPLD2 or carrying Ev. Seventy-two hours after the infection, MEFs were seeded on top of an SNL feeder layer in the presence of ES media, and the media was renewed every 24 h. Cell reprogramming and the acquisition of pluripotency were assessed by colony morphology, GFP expression and alkaline phosphatase activity assays to assess the effect of the gene of interest/condition of interest* on the efficiency of the reprogramming process and the acquisition of stem cell-like properties.

ATAC-seq

ATAC-seq assays were performed using standard protocols [31, 32], with minor modifications. Briefly, 70,000 ovarian cancer cells overexpressing PLD2 carrying shPLD2 or carrying Ev growing under normoxic or hypoxic conditions were collected by centrifugation for 5 min at 500 g 4 °C. The supernatant was removed, and the cells were washed with PBS. Then, the cells were lysed in 50 µl of lysis buffer (10 mM Tris-HCl pH 7.4, 10 mM NaCl, 3 mM $MgCl_2$, 0.1% NP-40, 1x Roche Complete protease inhibitors cocktail) by pipetting up and down. The whole cell lysate was used for TAGmentation, which was centrifuged for 10 min at 500 g 4 °C, resuspended in 50 µl of the Transposition Reaction containing 2.5 µl of Tn5 enzyme and TAGmentation Buffer (10 mM Tris-HCl pH 8.0, 5 mM MgCl2, 10% w/v dimethylformamide), and incubated for 30 min at 37 °C. Immediately after TAGmentation, DNA was purified using a Minelute PCR Purification Kit (Qiagen) and eluted in 20 µl. Libraries were generated by PCR amplification using NEBNext High-Fidelity 2X PCR Master Mix (NEB). The resulting libraries were multiplexed and sequenced in a HiSeq 4000 paired-end lane, producing 100 M 49-bp paired-end reads per sample.

Quantification and statistical analysis

All statistical analyses were performed using GraphPad Prism 4. The distribution of the quantitative variables among different study groups was assessed using parametric (Student's *t test*) or nonparametric (Kruskal–Wallis or Mann–Whitney) tests as appropriate. The experiments were performed a minimum of three times and were performed in independent triplicates each time. The survival data from the patient databases were analyzed by a log-rank Mantel–Cox statistical test.

Analyses of cancer patient databases

We performed meta-analyses using the R2 Genomics analysis and visualization platform (http://hgserver1.amc.nl) to analyze the *PLD2* mRNA expression levels in tumor and non-tumor ovarian samples from the databases. The statistical significance of the tumor versus normal samples was assessed ($P<0.05$). Patient survival was analyzed using an R2 Genomics analysis and visualization platform (http://hgserver1.amc.nl), which was developed by the Department of Oncogenomics of the Academic Medical Center (Amsterdam, Netherlands). Kaplan–Meier plots showing patient survival were generated using the databases with available survival data with the scan method, which searches for the optimum survival cut-off based on statistical analyses (log-rank test), thereby identifying the most significant expression cut-off.

ATAC-seq data analyses

ATAC-seq reads were aligned to the GRCh38 (hg38) human genome assembly using Bowtie2 2.3.5 [33], and pairs separated by more than 2 kb were removed. For ATAC-seq, the Tn5 cutting site was determined as position −4 (minus strand) or +5 (plus strand) from each read start, and this position was extended 5 bp in both directions. Reads below 150 bp were considered nucleosome free. The conversion of the SAM alignment files to BAM was performed using SAMtools 1.9 [34]. The conversion of BAM to BED files and peak analyses, such as overlaps or merges, were carried out using the Bedtools 2.29.2 suite [35]. The conversion of BED to BigWig files was performed using the genomecov tool from Bedtools and the wigToBigWig utility from UCSC [36]. For ATAC-seq, peaks were called using the MACS2 2.1.1.20160309 algorithm [37] with an FDR < 0.05 for each replicate and merged into a single pool of peaks that was used to calculate the differentially accessible sites with the DESeq2 1.18.1 package in R 3.4.3 [38]; a P value < 0.05 was set as the cut-off for statistical significance of the differential accessibility. For visualization purposes, reads were extended 100 bp for ATAC-seq. For the data comparison, all ATAC-seq experiments used were normalized using reads falling into peaks to counteract differences in background levels between experiments and replicates [39].

Heatmaps, average profiles and k-means clustering of the ATAC-seq data were generated using the computeMatrix and plotHeatmap tools from the Deeptools 3.5 toolkit [40]. The TF motif enrichment was calculated using XSTREME [41] with the standard parameters. For the gene assignment to ATAC peaks, we used the GREAT 3.0.0 tool [42], with the basal plus extension association rule and the standard parameters (5 kb upstream, 1 kb downstream, and 1 Mb maximum extension). For the footprinting analyses, we used TOBIAS 0.12.9 [43]. First, we performed bias correction using ATACorrect and calculated the footprint scores with ScoreBigwig, both with the standard parameters. Then, we used BINDetect to determine the differential TF binding of all vertebrate motifs in the JASPAR database [44]. We considered motifs with a linear fold-change ≥ 15% between conditions differentially bound. Aggregated ATAC-seq signals in the footprints were visualized using PlotAggregate. ATAC-seq data generated in this study is available through the Gene Expression Omnibus (GEO) accession number GSE210599.

In vivo xenograft studies

Tumor growth was assayed following the subcutaneous injection of 4×10^6 SKOV3 or OVCAR8 cells that were transfected with a plasmid carrying PLD2 or shRNA against *PLD2* in cohorts of five nude mice each that were analyzed weekly. The tumors were measured using callipers. All mice were sacrificed once the growth experiment was completed.

In vivo xenograft treatment

Tumors were harvested when they reached 1500 mm^3, cut into 2×2×2 mm pieces and reimplanted. Mice were randomly allocated to the drug-treated and control-treated (solvent only) groups, and once the tumor reached 20 mm^3, the mice received the appropriate treatment for 4 weeks (2 doses/week). The mice were monitored daily for signs of distress and weighed twice a week. The tumor size was measured, and the size was estimated according to the following equation: tumor volume = [length x $width^2$]/2. The experiments were terminated when the tumor reached 350 mm^3 or when the clinical endpoint was reached. The drugs cisplatin and carboplatin were obtained from Pharmacy HUVR and were freshly prepared and administered by intraperitoneal injection. We used higher doses in mice, assuming a 70 kg average weight for humans (125 mg/dose in humans) [28]. We administered two doses per week as follows: 3.5 mg/kg of cisplatin (equivalent to 7 mg/kg, averaging 25 g body weights of each mouse) with or without 3 mg/kg of FIPI. We did not observe signs of toxicity.

In vivo xenografts from tumorspheres

This assay involved the subcutaneous injection of 1×10^3 cells grown as tumorspheres into the hind legs of 4-week-old female athymic nude mice. The animals were treated as previously described, examined twice a week, incubated for 4 more weeks, and killed, and the tumors were extracted. The tumors were measured using callipers.

Patient cohort

The entire procedure was approved by the local ethical committee of the HUVR (CEEA O309-N-15). A cohort

of paraffin-embedded tissue samples from 25 patients with ovarian cancer was obtained from the biobank of Hospital Universitario Virgen del Rocío-Instituto de Biomedicina de Sevilla (Sevilla, Spain) for the RNA expression studies and the evaluation of the correlation of the clinicopathological features (see Supplementary Table S2, Additional File 1). The samples were obtained from biopsies of patients who were subjected to platinum treatment and who were evaluated for their response according to the RECIST criteria; normal tissue, platinum-resistant tumor samples and platinum-sensitive tumor samples were obtained. The tumor samples were sent to the pathology laboratory for diagnosis and were prepared for storage with formalin fixation and paraffin embedding. The samples were stained with haematoxylin/eosin, and RNA was extracted from the tumor tissue.

Results

PLD2 is overexpressed in OC patients and in ovarian cancer cells under hypoxic conditions

First, we wondered whether PLD2 was overexpressed in OC patients. For this, we analysed *PLD2* expression in 7 OC and one ovarian tissue databases using the R2 platform and found that *PLD2* expression was significantly higher in tumoral than in non-tumoral samples (Fig. 1A). This result was confirmed by a comparison between patients and control individuals in 3 databases containing their own controls (GSE18520, GSE4595 and GSE3866) (Fig. 1B), and was independent on the OC subtype (Supplementary Figure S1A-B, Additional File 1). Next, we assessed whether *PLD2* expression was associated with patient survival by analysing 4 OC databases with available overall survival (OS) data (GSE13876, GSE19161, GSE23554 and GSE31245). We split patients based on *PLD2* expression and found that the group with high *PLD2* expression had a significantly lower survival in the GSE19161 database (Fig. 1C). Similar but non-significant trends were observed in GSE13876, GSE23554 and GSE31245 (Supplementary Figure S1C, Additional File 1). Conversely, when we split patients in low-risk and high-risk based on their OS, we observed higher *PLD2* expression in high-risk patients (Supplementary Figure S1D, Additional File 1), indicating that *PLD2* is commonly overexpressed in OC patients and may be associated with decreased patient survival. Additional analyses using all available OC patient data in Kaplan-Meier plotter showed that both progression-free survival (PFS) and post-progression survival (PPS) were significantly lower in HGSOC patients with low *PLD2* expression compared with the high expression group, and PPS was also significantly lower when considering all OC subtypes (Supplementary Figure S1E, Additional File 1), although no differences in OS were detected. Altogether, these data indicate that *PLD2* is commonly overexpressed in OC patients and may be associated with both decreased patient progression free survival and/or disease progression.

Similar to other solid tumors, OC shows hypoxic areas, and its main dissemination site, the ascitic fluid, is also characterized by hypoxia [12]. Since *PLD2* expression is increased under hypoxic conditions in colon cancer cells [45] and is involved in tumor stemness through communication with the microenvironment in colorectal cancer [27], we investigated whether hypoxia could increase the expression of *PLD2* in OC. For this, we selected three human OC cell lines representative of the most common subtypes of OC: SKOV3, which is an epithelial ovarian serous cystadenocarcinoma cell line; OVCAR8, which is a high grade serous ovarian adenocarcinoma cell line; and ES-2, which is a human ovarian clear cell adenocarcinoma cell line. We found that *PLD2* expression was similar among the three cell lines and that oxygen levels of 3% led to a 2-fold increase in the expression of *PLD2* in all of them, while the well-known hypoxia target genes *LDHA* and *VEGFA* showed a similar increase, validating the results (Fig. 1D). The hypoxia-induced increase in PLD2 expression was also observed at the protein level by performing immunofluorescence in the three OC cell lines (Fig. 1E). In addition, we further demonstrated these findings by using the HIF-hydroxylase inhibitor DMOG, which increases HIF levels, generating a hypoxia-like phenotype under normoxic conditions (Supplementary Figure S2A-B, Additional File 1). Thus, we treated OC cells with DMOG and found that this treatment resulted in a similar increase in hypoxia marker gene expression as that induced by hypoxia, also leading to the observed increase in *PLD2* expression at both the mRNA and protein levels (Fig. 1D-E). Therefore, we can conclude that *PLD2* expression is promoted by hypoxia.

HIF-1α activates *PLD2* transcription through HREs at promoter and hypoxia-specific enhancer regions

We aimed to understand how hypoxia promotes *PLD2* expression. HIF-1α is considered the master transcriptional regulator of the cellular response to hypoxia. It forms a heterodimer with ARNT that binds HREs to control the expression of hypoxia-response genes [6]. To address the possibility that HIF-1α could regulate *PLD2* expression at the transcriptional level, we first searched for possible cis-regulatory elements (CREs) near the *PLD2* gene that may contain HREs. According to public 3D chromatin conformation experiments (micro-C) in human embryonic stem cells, the *PLD2* gene is located within a topologically associating domain (TAD) of 190 kb with a high interaction frequency at the 3D level and is relatively isolated from the neighbouring regions (Fig. 1F). To identify CREs that may regulate *PLD2* expression, we focused on a smaller region of 50 kb

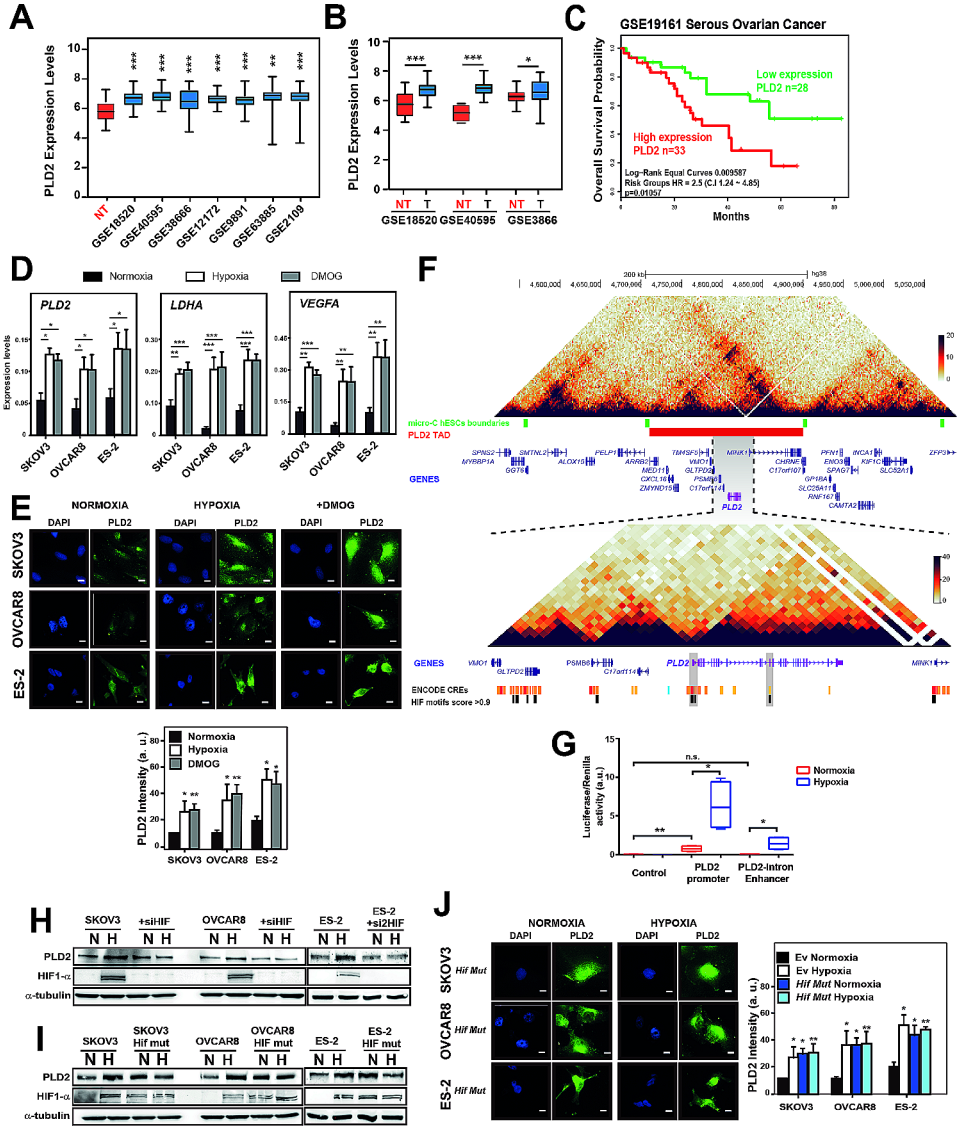

Fig. 1 Hypoxia leads to the overexpression of *PLD2* through HIF-1α in OC. (**A-B**) *PLD2* expression in OC patient databases. Box plots show *PLD2* expression as $\log_2$ transformed values from R2 database in ovarian tumor or non-tumor (NT) tissue. (**C**) Kaplan–Meier plot showing overall survival (OS) of patients with high or low *PLD2* expression in the database GSE19161. (**D**) *PLD2*, *LDHA* and *VEGFA* expression by RT-qPCR in SKOV3, OVCAR8 and ES-2 ovarian cancer cell lines under normoxia, hypoxia or treated with the HIF hydroxylase inhibitor DMOG. The mRNA expression was calculated as $2^{-\Delta Ct}$ relative to the *ACTB* gene. (**E**) Immunofluorescence and quantification of PLD2 protein levels in SKOV3, OVCAR8 and ES-2 cells carrying empty vector (Ev) under normoxia, hypoxia or treated with DMOG. Scale bars: 10 µm. (**F**) Top, heatmaps showing Micro-C signal in hESCs in a 0.5-Mb region of chromosome 17, TAD boundaries, the TAD containing *PLD2* gene and ENSEMBL genes. Bottom, zoom within the TAD containing the *PLD2* gene showing ENCODE cis-regulatory elements (CREs) and those containing HIF1 motifs with relative scores higher than 0.9. (**G**) Luciferase activity assay of *PLD2* promoter and putative enhancer in HEK293 cells under hypoxia or normoxia. (**H**) Western blot showing PLD2, HIF-1α and alpha-tubulin levels in SKOV3 or OVCAR8 cells with or without a small interfering RNA (siRNA) of HIF-1α. (**I**) Western blot showing PLD2, HIF-1α, and alpha-tubulin protein levels in SKOV3 and OVCAR8 cells expressing a *hif1a* mutant (HIF mut) or Ev. (**J**) Immunofluorescence and quantification of PLD2 protein levels in SKOV3, OVCAR8 and ES-2 cells carrying Ev or expressing Hif Mut under normoxia or hypoxia. Scale bars: 10 µm. At least three biological replicates were performed per experiment. Data were compared using Student's t tests. For D, E and G, asterisks indicate statistical significance compared with normoxia, and for J, compared with normoxia of cells carrying Ev. $^*p < 0.05$; $^{**}p < 0.01$; $^{***}p < 0.001$

surrounding the *PLD2* gene with a higher interaction frequency with the *PLD2* promoter, which we called the *PLD2* regulatory region. We scanned the CREs annotated by ENCODE within the *PLD2* regulatory region for the presence of the DNA binding motif of HIF1A with a high score (>90% relative score). We found 15 out of 35 CREs fulfilling this condition, some of which corresponded to gene promoters and others to enhancers, including the *PLD2* promoter and an enhancer in *PLD2* intron 12 (Fig. 1F). These CREs with high-score HIF1A motifs represent putative HREs.

To assess the regulatory activity of these two CREs in the *PLD2* gene (promoter and putative enhancer) containing the HIF1A motif, we cloned both genomic regions in promoter and enhancer reporter vectors controlling the expression of the luciferase gene. We transfected OC cells with these vectors and measured the luciferase activity under normoxia and hypoxia. We found that the *PLD2* promoter was able to activate reporter expression in normoxia and that hypoxia led to a significant increase in luciferase activity (8-fold) (Fig. 1G), suggesting that the *PLD2* promoter responds to hypoxic conditions by increasing *PLD2* transcription. However, the enhancer contained within the *PLD2* intron was unable to activate reporter expression in normoxia but led to a 22-fold increase in its expression in hypoxia (Fig. 1G), indicating that this enhancer acts as an HRE in OC cells.

Next, we wanted to validate functionally that the hypoxia-induced upregulation of *PLD2* expression was indeed mediated by HIF-1α. Therefore, we depleted *HIF1A* using a small interfering RNA (siRNA) in the three OC cell lines and found that it suppressed the increase in the PLD2 protein levels induced by hypoxia (Fig. 1H). Additionally, we generated *hif1a* mutant OC cell lines by transfecting cells with a mutant *hif1a* allele [46] that is unable to be hydroxylated and, therefore, is constitutively active even under normoxic conditions. Interestingly, we observed that the PLD2 levels in *hif1a* mutant cells were as high as those induced by hypoxia on a *HIF1α* wild-type background in both normoxia and hypoxia, confirming that HIF-1α activates PLD2 expression (Fig. 1I-J). Altogether, these data indicate that hypoxia induces *PLD2* expression in OC cells through transcriptional activation by HIF-1α at HREs in the *PLD2* gene.

Hypoxia alters the chromatin landscape of ovarian cancer cells in a PLD2-dependent manner

We examined whether *PLD2* expression mediated by HIF-1α could have an impact on hypoxia-induced gene regulation. For this, we first analyzed the effect of hypoxia and *PLD2* expression in the epigenomic landscape of OC cells through ATAC-seq experiments in SKOV3 cells under normoxia and hypoxia and altered *PLD2* expression under normoxia (*PLD2* overexpression) and hypoxia (*PLD2* depletion). We computationally called open chromatin regions (ATAC peaks) in normoxia and hypoxia and compared both conditions by a differential accessibility analysis; we detected 140 and 102 peaks with increased or decreased accessibility in hypoxia, respectively (Fig. 2A). The heatmaps and aggregate profiles of these differentially accessible regions (DARs) showed that the peaks with increased accessibility in hypoxia were also more open upon *PLD2* overexpression in normoxia, although to a lower extent, and vice versa, with the peaks showing decreased accessibility in hypoxia (Fig. 2B), suggesting that *PLD2* overexpression in normoxia has a similar effect on chromatin accessibility as hypoxia. Indeed, the DARs of EV- versus *PLD2*-overexpressing cells under normoxia showed similar changes in accessibility under hypoxia, reinforcing the previous idea (Supplementary Figure S3A-B, Additional File 1). Both DARs in normoxia versus hypoxia and control versus *PLD2* overexpression were associated with genes enriched in Gene Ontology terms related to the response to hypoxia or well-known functions of *PLD2*, respectively (Supplementary Figure S3C-D, Additional File 1). Moreover, changes in accessibility induced by hypoxia were suppressed by *PLD2* depletion (Fig. 2B), suggesting that the effect of hypoxia in chromatin accessibility is mediated by PLD2. Similarly, changes in accessibility upon *PLD2* overexpression in normoxia were absent in *PLD2*-depleted cells in hypoxia (Supplementary Figure S3B, Additional File 1), reinforcing the previous idea. Altogether, these data indicate that both hypoxia and *PLD2* overexpression induce similar alterations in the chromatin landscape of OC cells and that the effect of hypoxia is mediated by PLD2.

Next, we sought to investigate the possible mechanisms driving the alterations in the chromatin accessibility landscape induced by hypoxia and *PLD2* overexpression. For this, we first performed motif enrichment analyses of DARs. We found that DARs in hypoxia were enriched in the motifs of the AP-1, ETS and C2H2 zinc finger transcription factor families in the increased accessibility sites and the C2H2 zinc finger and fork head families in the decreased accessibility sites (Supplementary Figure S4A, Additional File 1). Similar enrichments were found in DARs upon *PLD2* overexpression (Supplementary Figure S4B, Additional File 1), reinforcing the idea of a similar effect under both conditions. To further elucidate the possible TFs involved in hypoxia and PLD2-mediated epigenomic changes, we estimated differential TF binding among the conditions based on footprints in ATAC-seq data. Using this approach, we confirmed the increased chromatin binding of AP-1 family transcription factors, such as FOS and JUN, consistent with their implication in the response to hypoxia [47]. (Fig. 2C-D). We also found other TF families showing increased TF binding in hypoxia, such as homeobox, paired box or fork head TFs, and the C2H2 zinc finger TF ZBTB32, while TF families with decreased binding in hypoxia included members of the bHLH, NF-Y and ETS families, among others (Supplementary Figure S4C, Additional File 1). When we compared these TFs with those showing increased binding upon *PLD2* overexpression in normoxia, we found that most of these TFs overlapped (Supplementary Figure S4C, Additional File 1). In particular, 25 TF motifs of the AP-1 family showed increased binding under both conditions. Interestingly, these AP-1

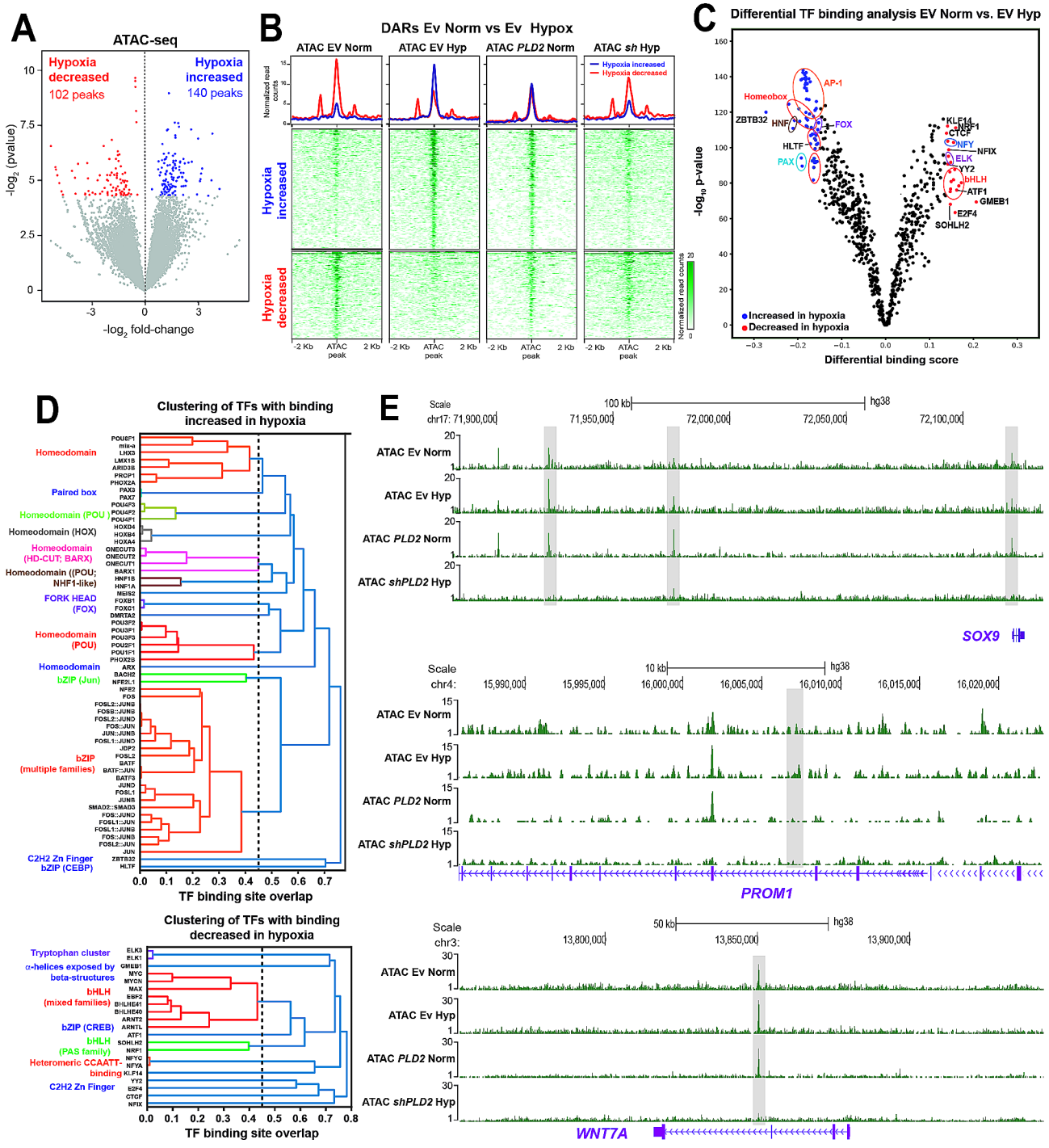

Fig. 2 Hypoxia and PLD2 modify the chromatin landscape of OC cells. (**A**) Differential analyses of accessibility between OC cells carrying Ev under normoxic or hypoxic conditions from ATAC-seq data ($n = 2$ biological replicates per condition). The log2 normalized read counts of peaks versus the log2-fold-change of accessibility are plotted. Peaks showing a statistically significant change (P value < 0.05) are highlighted in blue (hypoxia increased peaks) or red (normoxia increased peaks). (**B**) Heatmaps plotting normalized ATAC-seq signals at differentially accessible regions (DARs) from (f) in OC cells carrying Ev or expressing *PLD2* under normoxia and carrying Ev or expressing *shPLD2* under hypoxia. (**C**) Differential transcription factor (TF) binding analysis in OC cells carrying Ev under normoxia vs. hypoxia conditions using TOBIAS. Volcano plot showing the differential binding score versus the -$\log_{10}$ p value. TF motifs with increased (blue) or decreased (red) binding in hypoxia are highlighted. (**D**) Clustering of TFs with increased (top) or decreased (bottom) binding in hypoxia. (**E**) Tracks with ATAC-seq signals in OC cells carrying Ev in hypoxia or normoxia, expressing *PLD2* in normoxia or expressing *shPLD2* in hypoxia at the *SOX9, PROM1, and WNT7A loci*

and 20 more TF motifs with increased binding in hypoxia showed decreased binding upon *PLD2* depletion (Supplementary Figure S4C-E, Additional File 1), indicating that they are dependent on *PLD2* expression. Altogether, these results suggest a function of the AP-1 family of TFs mediating the alterations in the chromatin landscape mediated by hypoxia and PLD2.

Since we previously connected *PLD2* overexpression with tumor stemness in colorectal cancer, we analyzed whether alterations in the chromatin accessibility landscape of OC cells induced by hypoxia and PLD2 could result in increased expression of stemness genes. Therefore, we first selected ATAC peaks falling within the putative regulatory landscapes of the genes associated with stem cell maintenance and proliferation. Clustering of these 3,572 peaks revealed 4 groups with different accessibility levels and behaviours (Supplementary Figure S5A, Additional File 1). Among them, Cluster 3 corresponded with peaks with increased accessibility in both hypoxic and *PLD2*-overexpressing cells but decreased accessibility in *PLD2*-depleted cells. Among the stemness genes associated with this cluster, we found *SOX9*, *PROM1*, *WNT7A* or *JAG1* (Fig. 2E; Supplementary Figure S5B, Additional File 1). These results indicate that hypoxia promotes chromatin accessibility around stemness genes in a PLD2-dependent manner in OC cells, and suggests that hypoxia and PLD2 could be connected with tumor stemness in OC.

High *PLD2* expression in OC patients leads to the transcriptomic rewiring of stemness and hypoxia genes

To determine whether *PLD2* expression in OC patients is related to hypoxia and stemness, we analysed the expression of genes related to these functions in the three OC databases with available expression data from control individuals. First, we selected the genes annotated to the Gene Ontology (GO) term "Response to Hypoxia" and whose expression was significantly correlated with that of *PLD2* in OC patients ($p<0.05$; $r>0.2$ or <-0.2). Then, we performed hierarchical clustering of patient and control individuals based on the expression levels of these genes (Fig. 3A; Supplementary Figure S6, Additional File 1). In the GSE18520 database, the clustering clearly separated the control individuals ('non-tumoral', NT) and a reduced group of patients that we termed 'Tumoral Cluster 1' (T1) from most patients who clustered in what we termed 'Tumoral Cluster 2' (T2) (Fig. 3A). The patients at T1 showed a transcriptional profile of hypoxia-related genes more similar to NT and clearly different from T2. In contrast, the clustering in the GSE4095 and GSE38666 databases clearly separated clusters of NT and tumoral (T) individuals, who showed distinct transcriptional profiles of hypoxia-related genes (Supplementary Figure S6, Additional File 1). These results suggest that there is a switch in the expression of hypoxia-related genes in OC tumors compared with healthy ovaries.

Next, we repeated the hierarchical clustering with the genes annotated to the GO term "Stem cell maintenance" and whose expression was significantly correlated with that of *PLD2* in OC patients ($p<0.05$; $r>0.2$ or <-0.2). Surprisingly, this clustering based on stem-related genes separated the patients and control individuals into the same clusters as the hypoxia-related genes (Fig. 3A; Supplementary Figure S6, Additional File 1), suggesting a connection between both groups of genes that supports the model of CSC generation induced by hypoxia. Then, we plotted the expression levels of *PLD2* in the 3 clusters obtained from the GSE18520 database and found that *PLD2* exhibited significantly increased expression in Cluster T2 compared with that in Cluster NT, while Cluster T1 showed similar levels to NT (Fig. 3B). This observation suggests that a connection exists among *PLD2* expression, the hypoxia response and stemness since *PLD2* expression is misregulated only in patients showing transcriptional profiles highly different from healthy controls. In addition, we checked the expression of stem-associated and hypoxia-related genes in these clusters. As shown in Fig. 3B, the expression of *PAX8*, a well-known OC marker, was significantly increased in both patient Clusters T1 and T2, similar to other stemness genes, such as *SOX9*, *SOX17*, *EPCAM*, *PROM1*, *CD24*, *NOTCH1* and *WNT7A*. Other genes in this group showed a significant.

increase in expression only in Cluster T2, coinciding with higher *PLD2* levels, including *PAX2*, *POU5F1* (*OCT4*), *SOX5*, *SOX11*, *CD34* and *TP63*, while the others were unaffected or even significantly reduced, such as *KLF4*, *NANOG* or *SOX2*, although the latter showed a nonsignificant increase in Cluster T2 (Fig. 3B). This finding suggests that there is an OC stemness signature in patients that may be stronger with higher *PLD2* expression. In addition, some hypoxia-related genes showed a significant increase in expression in both Clusters T1 and T2, including *VEGFA*, *SLC2A1* (*GLUT1*), *HK2* and *NOX4*, or only in T2, including *SLC2A4*, *NOS1* and *MMP14*, and a nonsignificant increase in *SLC2A14* (*GLUT14*) (Fig. 3B). Similar results were obtained in the NT and T clusters in the GSE4095 and GSE38666 databases (Supplementary Figure S6, Additional File 1). Altogether, these results suggest that there is transcriptional rewiring of the expression of hypoxia- and stem-related genes in OC patients with *PLD2* overexpression.

PLD2 promotes tumorigenesis and CSC-like features in ovarian cancer cells

The ability of hypoxia to induce a CSC-like phenotype in OC cells has been previously observed in several cancer types [25, 26, 48]. We first aimed to validate these results in our OC cell lines SKOV3, OVCAR8 and ES-2

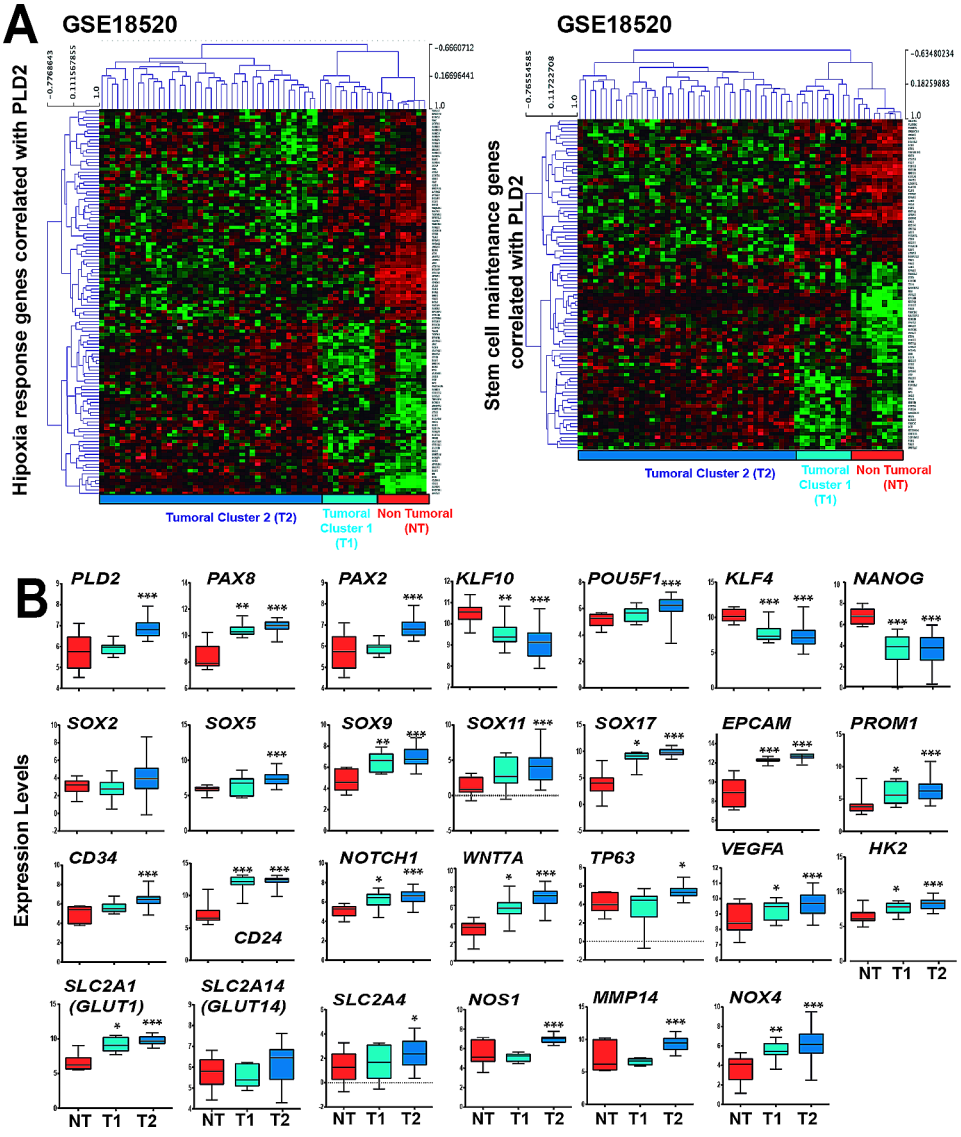

Fig. 3 High *PLD2* expression in OC patients leads to a transcriptomic rewiring of hypoxia and stemness genes. (**A**) Heatmaps showing the expression z scores of stem-associated genes or hypoxia response genes whose expression was correlated with *PLD2* in the GSE18520 OC patient database. (**B**) Expression levels of *PLD2* and selected stem-associated or hypoxia response genes correlated with *PLD2* in the OC patient database GSE18520. Box plots showing gene expression in patients in tumoral Cluster 1 (T1; light blue), tumoral Cluster 2 (T2; dark blue), or nontumor tissue (NT; red). Box plots representing the centreline, median; box limits, 25th and 75th percentiles. For B data were compared using Student's t tests. Asterisks indicate statistical significance with respect to NT tissue. *$p < 0.05$; **$p < 0.01$; ***$p < 0.001$

and found that hypoxia led to significant increases in the number of tumorspheres, which were generated by growing the cells under low-attachment conditions, and in the percentage of holoclones, both of which were used as a proxy for CSCs (Supplementary Figure S7A-B, Additional File 1). Next, we analysed the expression of stem cell markers in OC cell lines grown under hypoxic conditions and detected an increase in the mRNA levels of *NANOG*, *CD44*, *SOX2* and *EPCAM* and the percentage of cells containing the surface CSC marker CD133 (Supplementary Figure S7C-D, Additional File 1). These results confirm that hypoxia induces a CSC-like phenotype in OC cells.

Next, we investigated whether increased *PLD2* expression led to an increase in the CSC population in OC cells, as suggested by the chromatin accessibility and gene expression data. Therefore, we first established OC cell lines expressing ectopic *PLD2* cDNA or depleted of *PLD2* using a short hairpin RNA (shRNA). The expression of *PLD2* under these conditions was assessed at the mRNA and protein levels (Fig. 4A-B and Supplementary Figure S8, Additional File 1). We observed that the overexpression of *PLD2* in OC cells led to a significant increase in

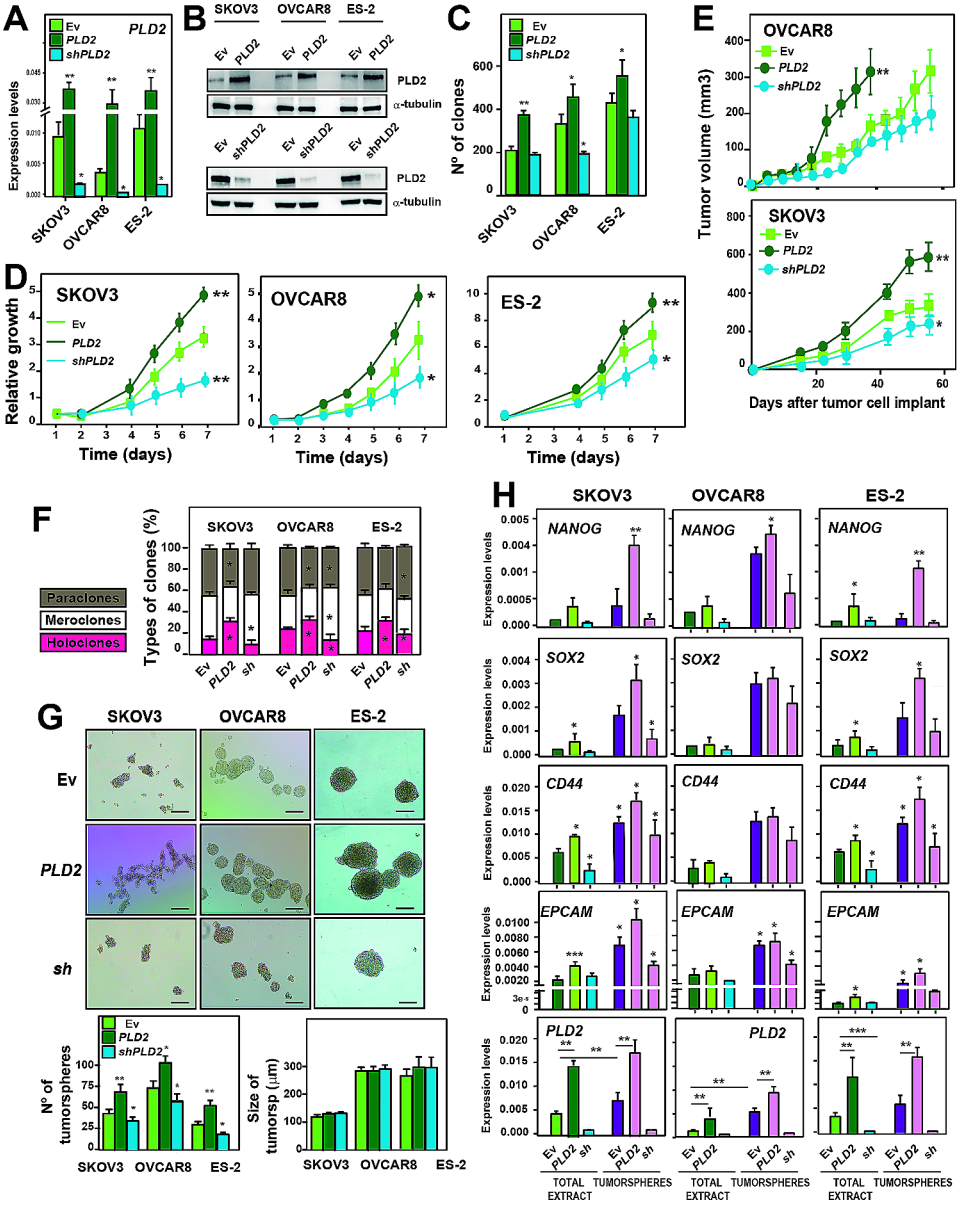

Fig. 4 *PLD2* promotes tumorigenesis and CSC-like features in ovarian cancer. (**A**) Analysis of the expression of *PLD2* by RT–qPCR in SKOV3, OVCAR8 and ES-2 cells carrying an empty vector (Ev) expressing *PLD2* or *shPLD2*. The mRNA expression was calculated as $2^{-\Delta Ct}$ relative to the *ACTB* gene. (**B**) Western blot showing the protein levels of PLD2 in cells carrying Ev and expressing *PLD2* or *shPLD2*. (**C**) Quantification of the number of colonies formed by SKOV3, OVCAR8 and ES-2 cells carrying Ev and expressing *PLD2* or *shPLD2*. **(D)** Growth curve of SKOV3, OVCAR8 and ES-2 cells carrying Ev (light green) or expressing *PLD2* (dark green) or *shPLD2* (blue) represented as the accumulation of the doubling times. **(E)** Tumor growth in xenografts from SKOV3 and OVCAR8 cells carrying Ev, overexpressing *PLD2* or *shPLD2* were injected into female athymic nude mice. Cohorts of 5 mice each were used. (**F**) Percentage of paraclones, meroclones and holoclones formed by SKOV3, OVCAR8 and ES-2 cells carrying Ev expressing *PLD2* or *shPLD2*. At least 200 individual clones were analysed. The averages and SDs of three independent experiments are shown. (**G**) Top, Representative images of tumorspheres formed by SKOV3, OVCAR8 and ES-2 cells carrying Ev expressing *PLD2* or *shPLD2*. Bottom, quantification of the number and size of tumorspheres. Scale bars: 250 µm. (**H**) Analysis of the expression by RT–qPCR of stemness-associated genes and *PLD2* in total cell extracts and tumorspheres from SKOV3, OVCAR8 and ES-2 cells carrying Ev and expressing *PLD2* or *shPLD2*. The mRNA expression was calculated as $2^{-\Delta Ct}$ relative to the *ACTB* gene. The average and SD of at least three independent experiments are shown. The data were analysed using Student's t test. Asterisks indicate statistical significance with respect to Ev carrying cells. *, $P < 0.05$; **, $P < 0.01$; ***, $P < 0.001$

the number of clones generated by the three cell lines, while a significant decrease was detected in the OVCAR8 cells upon *PLD2* depletion (Fig. 4C), suggesting that PLD2 promotes tumor growth. To address this question, we analysed the growth of these cell lines and found that the enhanced *PLD2* expression led to a significant increase in proliferation, while the *PLD2* depletion generated the opposite effect with statistical significance in

all cell lines (Fig. 4D). This effect was further confirmed in vivo by generating xenograft models of OC cells overexpressing or depleted of *PLD2*, showing an increase or decrease in the tumor volume, respectively, 50 days after transplantation (Fig. 4E). Altogether, these results indicate that *PLD2* expression promotes tumorigenesis.

Next, we assessed whether *PLD2* expression was related to the formation of ovarian CSCs. First, we analysed the formation of different types of colonies, including holoclones, meroclones and paraclones, which are considered stem cells, transit-amplifying cells and differentiated cells, respectively [30]. We found a significant increase in the percentage of holoclones in the three OC cell lines overexpressing *PLD2*, as well as a significant decrease in paraclone formation in SKOV3 and OVCAR8 cells and a similar but non-significant trend in ES-2 cells (Fig. 4F). In contrast, a significant decrease in holoclone formation upon *PLD2* depletion was observed in OVCAR8 and ES-2 cells, and a similar non-significant trend in SKOV3 cells (Fig. 4F). Furthermore, we measured the formation of tumorspheres under low attachment conditions in OC cells overexpressing or depleted of *PLD2*. We found that *PLD2* overexpression led to a significant increase in the number of tumorspheres, while *PLD2* depletion generated the opposite effect (Fig. 4G), although we did not observe changes in the size of such tumorspheres. These data indicate that *PLD2* expression promotes the formation of ovarian CSCs.

Finally, we analysed the expression of pluripotency and CSC marker genes in our OC cell lines overexpressing or depleted of *PLD2*. We found that the expression of.

SOX2, *CD44* and *EPCAM* was significantly increased in the ES-2 and SKOV3 cells overexpressing *PLD2*, while *NANOG* was only increased in ES-2 cells (Fig. 4H). In OVCAR8 cells, the expression of these genes was increased in the same trend, although in a nonsignificant manner. Then, we measured the expression levels of these pluripotency genes in the tumorspheres extracts. First, we found that *PLD2* was highly expressed in the tumorspheres compared with that in the total extracts transfected with only the empty vector (Fig. 4H), confirming that CSCs indeed have higher expression levels of *PLD2*. The expression of stemness genes was also increased in the tumorspheres compared with that in the total extracts, as expected, while they were further upregulated in most cases upon *PLD2* overexpression, or downregulated upon *PLD2* depletion (Fig. 4H). Altogether, these data indicate that *PLD2*, whose expression is induced by hypoxia, is an important oncogene in OC and that its overexpression leads to increased tumor stemness.

The hypoxia-induced stemness of ovarian cancer cells partially depends on *PLD2* expression

Thus far, we have showed that both hypoxia and *PLD2* expression led to an increase in CSCs in OC cells (Fig. 4, Supplementary Figure S7, Additional File 1) and that *PLD2* expression was increased under hypoxic conditions in a HIF-1α-dependent manner (Fig. 1). Thus, we evaluated whether both phenomena were connected and whether the hypoxia-induced increase in CSC-like features was dependent on *PLD2* expression. To address this, we first analysed the expression levels of stemness genes by RT−qPCR using custom TaqMan Array plates containing probes against a selection of these genes in OC cells. We observed that either hypoxia or *PLD2* overexpression in normoxia led to the increased expression of many stemness genes, while *PLD2* depletion largely suppressed this increase (Fig. 5A). Indeed, hierarchical clustering of the four analysed conditions showed that the samples corresponding to EV hypoxic cells and *PLD2*-overexpressing cells clustered together, while EV normoxic cells and *PLD2*-depleted cells clustered separately (Fig. 5B). We confirmed these result by RT−qPCR of individual representative genes, including *SOX2*, *NANOG*, *CD44* and *EPCAM*, showing that either hypoxia or *PLD2* overexpression in normoxia lead to increased expression of stemness genes, while combination of both conditions further increased their expression (Fig. 5C). *PLD2* depletion partially suppressed the hypoxia-induced enhancement of expression, with a lower non-statistically significant effect in normoxia, and rescue experiments confirmed the specificity of *PLD2* depletion (Fig. 5C).

Next, we analyzed the formation of tumorspheres in normoxia and hypoxia with altered *PLD2* expression. We observed that either *PLD2* overexpression or hypoxia led to a similar increase in the formation of tumorspheres, with only a slightly higher nonsignificant increase when both conditions were combined (Fig. 5D). However, *PLD2* depletion caused a partial suppression of the increase in tumorsphere formation under hypoxic conditions in SKOV3 and OVCAR8 cells, which was rescued by overexpressing back *PLD2* in shRNA-transfected cells (Fig. 5D and Supplementary Figure S9A, Additional File 1), suggesting that PLD2 is partially responsible for the hypoxia-induced stemness. Then, we measured the formation of holoclones, meroclones and paraclones under hypoxic conditions upon *PLD2* overexpression or depletion and found that the increase in the percentage of holoclones induced by hypoxia was further enhanced by the *PLD2* overexpression, while it was suppressed by *PLD2* depletion and rescued back by expressing *PLD2* after its depletion (Supplementary Figure S9B, Additional File 1).

Then, we measured the protein levels of the pluripotency factors Sox2, Sox17, Sox9 and Notch1 (found to

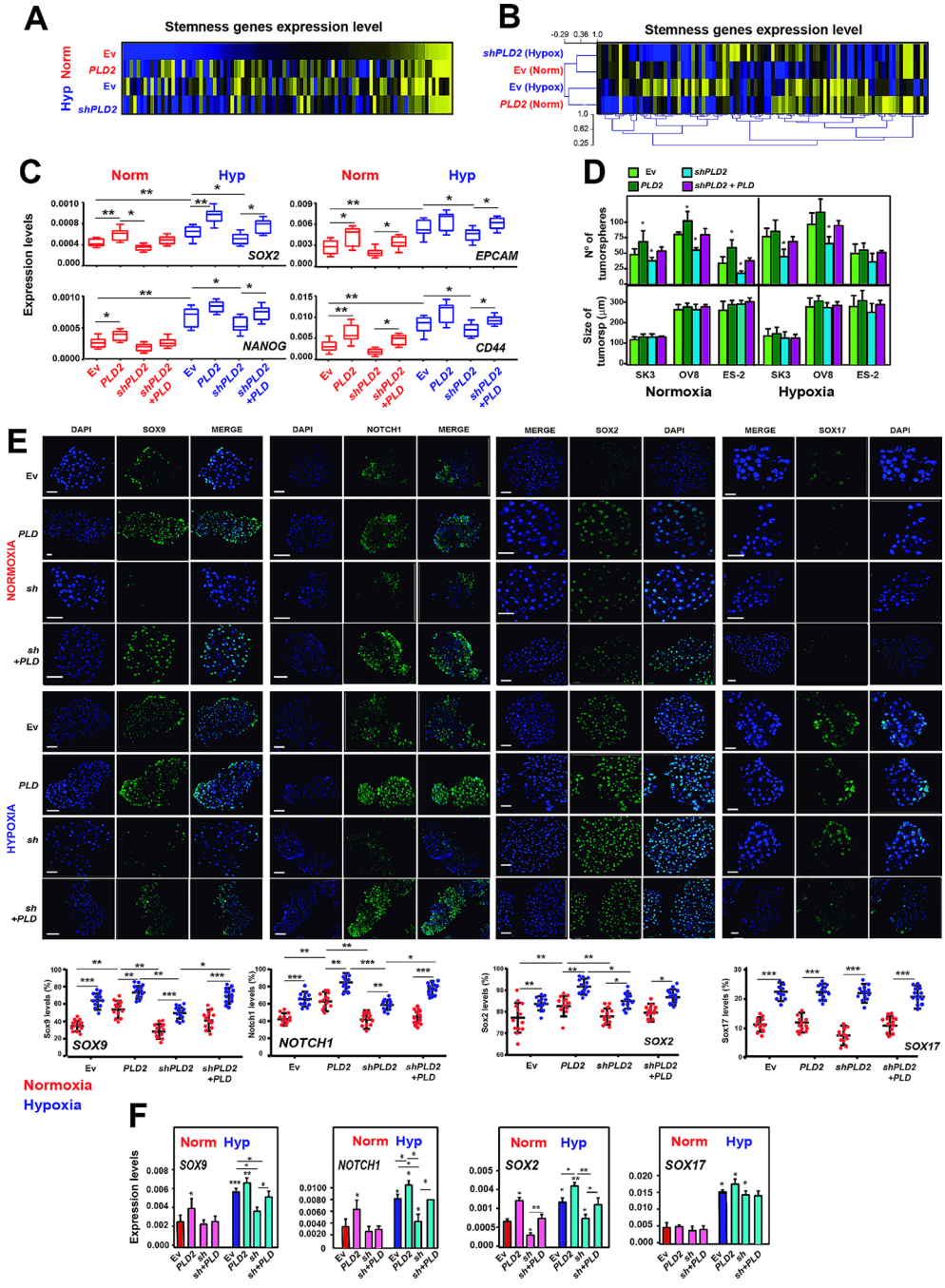

Fig. 5 The hypoxia-induced stemness of OC cells depends on *PLD2* expression. (**A**) Heatmaps showing the z scores of the expression of stemness-associated genes obtained from TaqMan arrays. Genes are sorted according to decreasing z scores in Ev-carrying cells under normoxia. (**B**) Heatmaps showing the z-scores of stemness genes expression levels in SKOV3 cells carrying EV or plasmid overexpressing *PLD2* under normoxia and carrying EV or plasmid expressing *shPLD2* under hypoxia. Hierarchical clustering of the samples of (A) is shown. (**C**) Expression levels of *SOX2, NANOG, CD44* and *EPCAM* stemness-associated genes in SKOV3, OVCAR8 and ES-2 cells carrying Ev and expressing *PLD2*, *shPLD2* or both under normoxic or hypoxic conditions. The mRNA expression was calculated as $2^{-\Delta Ct}$ relative to the *ACTB* gene. (**D**) Quantification of the number and size of tumorspheres formed by SKOV3, OVCAR8 and ES-2 cells carrying Ev and expressing *PLD2*, *shPLD2* or both. (**E**) Top, determination of the Sox9, Notch1, Sox2, and Sox17 protein levels by immunofluorescence in tumorspheres formed by OC cell lines carrying Ev and expressing *PLD2*, *shPLD2* or both. Bottom, quantification of the percentage of cells with Sox9 and Notch1 expression in tumorspheres formed by ovarian cancer cell lines carrying Ev and expressing *PLD2* or *shPLD2*. Scale bars: 100 µm. **(F)** Expression levels of *SOX9, NOTCH1, SOX2* and *SOX17* stemness-associated genes in tumorspheres formed by ovarian cancer cell lines carrying Ev and expressing *PLD2*, *shPLD2* or both. The mRNA expression was calculated as $2^{-\Delta Ct}$ relative to the *ACTB* gene. A minimum of three biological were performed per each experiment. The data were analysed using Student's t test. Asterisks indicate statistical significance with respect to Ev carrying cells, unless indicated by horizontal lines. *, $P < 0.05$; **, $P < 0.01$; ***, $P < 0.001$

correlate with PLD2 in OC patients, Fig. 3B) by immunofluorescence in tumorspheres to determine whether PLD2 could influence their expression in CSCs. We validated PLD2 protein levels in tumorspheres (Supplementary Figure S9C, Additional File 1) and found that either hypoxia or *PLD2* overexpression led to an increase in the levels of Sox2, Sox9 and Notch1, while only hypoxia led to an increase in Sox17 protein levels (Fig. 5E). In addition, *PLD2* depletion led to a partial suppression of the hypoxia-induced expression of Sox2, Sox9 and Notch1 that was rescued by expressing back *PLD2* in these cells (Fig. 5E), suggesting that PLD2 plays a role in the generation of CSCs in hypoxia through these genes. These observations were confirmed at the mRNA level by RT–qPCR (Fig. 5F). Altogether, these data indicate that PLD2 plays a major role in the induction of the CSC phenotype in hypoxia, promoting the expression of specific stem-related genes, such as *SOX2*, *SOX9* or *NOTCH1*.

Finally, we extended the gene expression analyses to EMT genes using TaqMan Arrays to assess whether *PLD2* expression may have a role in tumor invasion and metastasis. We found that either hypoxia or *PLD2* overexpression in normoxia led to an increase in the expression of many of these genes, but *PLD2* depletion was unable to suppress such increase (Supplementary Figure S10A, Additional File 1). Indeed, hierarchical clustering of the samples did not exhibit the pattern observed in stemness genes (Supplementary Figure S10B, Additional File 1), and results were further validated by RT–qPCR of particular EMT genes (Supplementary Figure S10C, Additional File 1). Consistently, invasiveness assays using Boyden's chamber showed that both *PLD2* overexpression and hypoxia were able to increase invasion, but *PLD2* depletion did not have any effect (Supplementary Figure S10D, Additional File 1). These results indicate that while the increased expression of stemness genes induced by hypoxia relies on *PLD2* overexpression, this is not the case for EMT genes and suggests that PLD2 is a specific mediator of the increase in CSCs induced by hypoxia in OC cells.

Hypoxia-mediated reprogramming to induced pluripotent stem cells is dependent on PLD2

We aimed to obtain additional evidence of the contribution of PLD2 to dedifferentiation or reprogramming events mediated by hypoxia that may generate ovarian CSCs from normal OC cells. Therefore, we performed reprogramming experiments of mouse embryonic fibroblasts (MEFs) to induced pluripotent stem cells (iPSCs) in normoxia and hypoxia and upon alteration of *PLD2* expression levels (overexpression or depletion). We used a previously published protocol [49] in which MEFs were infected using a HEK293T cell-derived virus that provides OSKM genes and Nanog reporter retroviruses and then cocultured on SNL feeder cells that produce LIF. Then, the samples were incubated with or without hypoxia for 7 days, and the efficiency of iPSC generation was measured for additional 5 days. Cell reprogramming and the acquisition of pluripotency were assessed by colony morphology, alkaline phosphatase and *nanog* promoter-driven GFP expression analyses (Fig. 6A) to assess the effect of PLD2 and hypoxia on the efficiency of the reprogramming process and the acquisition of stem cell-like properties. Using this protocol, we found that, as expected, hypoxia led to a significant increase in the generation of iPSCs (Fig. 6B). Furthermore, we found that *PLD2* overexpression in normoxia provoked a similar increase in iPSC generation, consistent with its effect on the generation of CSCs, and that the combination of both hypoxia and *PLD2* overexpression further increased iPSC

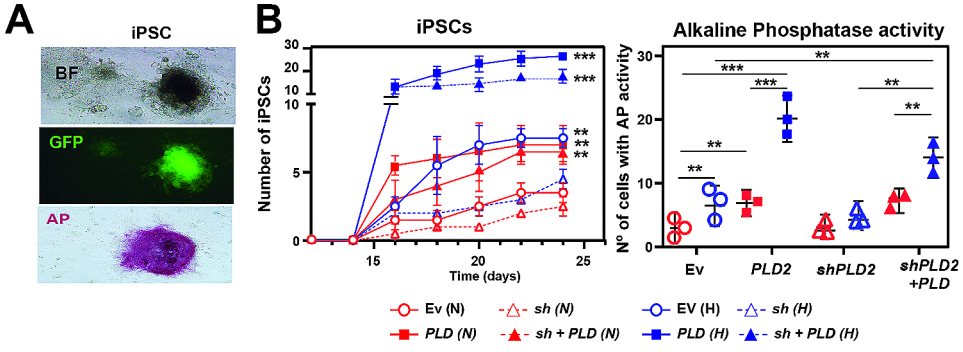

Fig. 6 Hypoxia-mediated reprogramming to pluripotent stem cells is dependent on PLD2. (**A**) Representative images of induced pluripotent stem cells (iPSCs) by reprogramming mouse embryonic fibroblasts (MEFs) with OSKM genes (Yamanaka factors Oct3/4, Sox2, Klf4 and cMyc) and Nanog reporter retroviruses. Top, bright field microscopy of iPSCs. Medium, immunofluorescence image showing GFP in cells in which *Nanog* is active. Bottom, Alkaline phosphatase activity. (**B**) Left, quantification of iPSCs generated from MEFs infected with OSKM genes and an additional lentiviral vector that expresses GFP in cells in which the Nanog promoter/enhancer is active and the corresponding plasmid overexpressing *PLD2*, *shPLD2*, both or carrying Ev under normoxia or hypoxia. Right, quantification of cells with alkaline phosphatase activity at the end of the iPSC generation experiment. A minimum of three biological were performed per each experiment. The data were analysed using Student's t test. Asterisks indicate statistical significance with respect to Ev carrying cells, unless indicated by horizontal lines. *, $P < 0.05$; **, $P < 0.01$; ***, $P < 0.001$

formation (Fig. 6B). This confirms that high *PLD2* expression leads to dedifferentiation processes. Finally, *PLD2* depletion in hypoxia suppressed the increased iPSC production induced by hypoxia, and this was recovered by expressing back *PLD2* in *PLD2*-depleted cells (Fig. 6B), suggesting that PLD2 is an important mediator in the activation of pluripotency by hypoxic conditions.

Overexpression of *PLD2* leads to chemotherapy resistance in ovarian tumors

Since we showed that *PLD2* overexpression leads to an increase in CSC-like cells in OC and CSCs were previously proposed to be responsible for chemotherapy resistance and tumor relapse, we wondered whether *PLD2* overexpression could cause resistance to conventional therapy in ovarian tumors. Therefore, we first analysed the expression levels of *PLD2* in our own cohort of OC patients. The immunohistochemistry analyses showed that *PLD2* protein levels were higher in tumors than in healthy tissue (Fig. 7A), and RT−qPCR revealed that *PLD2* mRNA was significantly more abundant in OC patients than in control non-tumoral samples (Fig. 7B), thus confirming the results observed in the transcriptomic databases (Fig. 1A-B). Then, we separated our patient samples into those who were sensitive or resistant to platinum-based chemotherapy (without or with tumor relapse within the next 6 months after chemotherapy, respectively) and analysed *PLD2* expression levels. Importantly, we found that the resistant patients showed significantly higher expression of *PLD2* than the sensitive patients (Fig. 7C), and this difference was higher when considering only HGSOC patients (Fig. 7D) suggesting that *PLD2* overexpression may contribute to resistance to platinum-based therapy. Resistant patients in our cohort showed reduced OS and PFS (Fig. 7E-F), consistent with the reduced survival of patients with high *PLD2* expression (Fig. 1C).

Next, we analyzed the effect of *PLD2* expression on resistance to platinum compounds in OC cells in vitro. First, cells overexpressing or depleted of *PLD2* in normoxia were treated with increasing concentrations of cisplatin and carboplatin, and the IC_{50} values were calculated in each case. We found that *PLD2* overexpression led to a significant increase in the IC_{50} values, while *PLD2* depletion led to only a weak nonsignificant reduction (Fig. 7G-H), indicating that high *PLD2* expression increases resistance to platinum compounds in OC cells. Then, we performed these experiments with low oxygen and found that hypoxia led to increased IC_{50} values in Ev-carrying cells (Fig. 7G-H). Furthermore, *PLD2* depletion in hypoxia reduced IC_{50} values compared with Ev-carrying cells in the same conditions, for all cell lines treated with either cisplatin or carboplatin (Fig. 7G-H). These results suggest that enhanced resistance of OC cells to platinum-based compounds induced by hypoxia is dependent on *PLD2* expression.

Finally, we performed in vivo analyses to validate our findings by establishing xenograft models from SKOV3 and OVCAR8 cells overexpressing *PLD2* or parental cells and analyzing tumor growth upon treatment with cisplatin. The control tumors from cells transfected with the empty vector were sensitive to the cisplatin treatment, significantly reducing tumor growth in xenografts from both SKOV3 and OVCAR8 cells (Fig. 7I). However, tumors overexpressing *PLD2* showed higher tumor growth that was not reduced upon cisplatin treatment, indicating both a higher aggressiveness of *PLD2*- overexpressing tumors and the resistance of these tumors to cisplatin (Fig. 7I). Furthermore, cisplatin treatment in control tumors led to increased survival, while *PLD2*-overexpressing tumors did not exhibit improved survival with cisplatin treatment (Fig. 7J). These results indicate that the overexpression of *PLD2* causes resistance to platinum-based chemotherapy in OC tumors.

Combination treatment with cisplatin and a PLD inhibitor suppresses chemotherapy resistance in ovarian cancer

Finally, we wondered whether the increased therapy resistance to platinum-based compounds induced by *PLD2* overexpression and hypoxia could be suppressed by the pharmacological inhibition of PLD2 in vivo. For this, we used the PLD inhibitor (PLDi) 5-Fluoro-2-indolyl des-chlorohalopemide (FIPI), which inhibits the catalytic activity of phospholipases D ([50]). First, we tested this possibility in vitro by calculating the IC_{50} in OC cells treated with cisplatin, PLDi and their combination in normoxia and hypoxia with altered levels of *PLD2*. We found that the higher IC_{50} to cisplatin of OC cells overexpressing *PLD2* or growing in hypoxia was suppressed by the PLDi (Fig. 7H). Next, we validated these results in vivo by establishing xenografts of OC cells carrying EV or overexpressing *PLD2* and treating mice with cisplatin, PLDi or their combination. We found that the increased tumor growth provoked by *PLD2* overexpression was reduced upon treatment with PLDi (Fig. 7I). Moreover, although treatment with cisplatin alone did not reduce the higher tumor growth induced by *PLD2* overexpression, its combination with PLDi led to a further reduction in tumor growth (Fig. 7I). This finding was confirmed in xenografts from both OVCAR8 and SKOV3 cells. Finally, combination treatment with cisplatin and PLDi led to an increase in the survival of mice carrying xenografts from *PLD2*-overexpressing cells (Fig. 7J). Altogether, these results indicate that chemotherapy resistance to cisplatin caused by *PLD2* overexpression can be overcome by the pharmacological inhibition of PLD2, suggesting that combined treatment with cisplatin and PLDi is

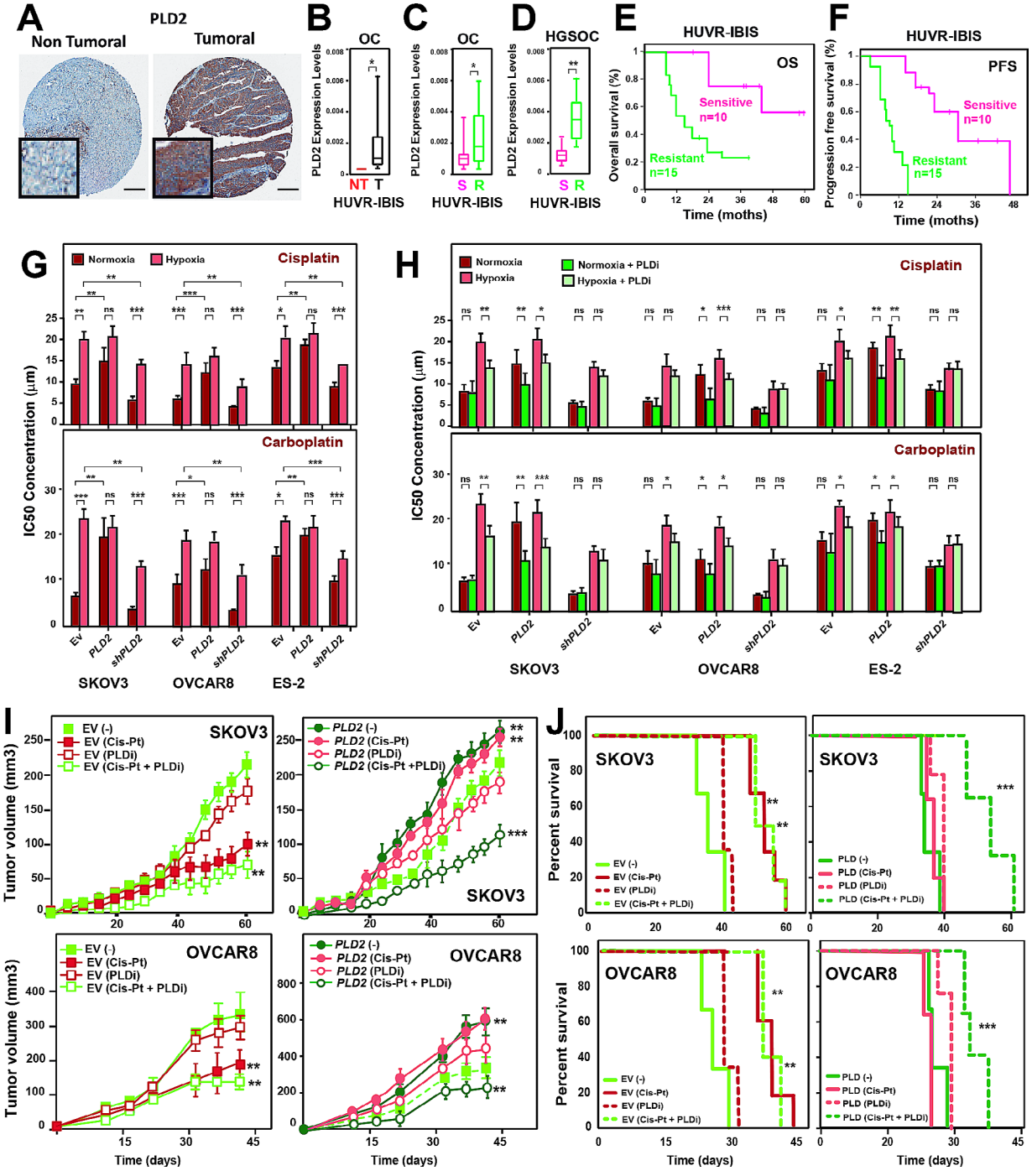

Fig. 7 *PLD2* overexpression is associated with resistance to treatment in ovarian cancer. (**A**) Representative images of PLD2 immunostaining in ovarian cancer and non-tumoral samples. Scale bars, 200 µm. (**B**) *PLD2* expression in ovarian patients from the HUVR-IBIS database. Box plots showing the *PLD2* expression levels in ovarian tumor tissue (black) or nontumor tissue (red) from patients. Box plots representing the centre line, median; box limits, 25th and 75th percentiles; whiskers, minimum and maximum values. (**C**-**D**) Analysis of *PLD2* expression by RT–qPCR in a cohort of (**C**) OC patients or (**D**) only HGSOC patients who were sensitive (S; pink) or resistant (R; green) to platinum treatment (HUVR-IBIS). For B and C, the mRNA expression was calculated as $2^{-\Delta Ct}$ relative to the *ACTB* gene. (**E**-**F**) Kaplan–Meier plots showing overall or progression-free survival in patients who were sensitive (pink) or resistant (green) to platinum treatment in the HUVR-IBIS cohort. (**G**-**H**) Determination of the IC_{50} of cis-platinum and carboplatin in ES-2, SKOV3 and OVCAR8 cells overexpressing *PLD2* or *shPLD2* or carrying EV in (**G**) normoxia and hypoxia, (**H**) in combination or without the PLD inhibitor (PLDi) FIPI in ES-2, SKOV3 and OVCAR8 cells overexpressing *shPLD2* or *PLD2* or carrying EV in normoxia or hypoxia. (**I**-**J**) Determination of the tumor volume (**I**) and survival (**J**) after treatment with saline (-), cisplatin (Cis-Pt), the PLD inhibitor FIPI (PLDi) or both (Cis-Pt + PLDi) in xenografts of SKOV3 or OVCAR8 cells expressing *PLD2* or EV. A minimum of three biological were performed per each experiment. The data were compared using Student's t tests. *$p < 0.05$; **$p < 0.01$; ***$p < 0.001$

a promising alternative treatment for patients with high *PLD2* expression levels.

Discussion

We show here that the HIF-1α-PLD2 axis is a major player in the chemoresistance of OC by promoting the generation of CSCs under hypoxic conditions. On the one hand, *PLD2* expression is regulated by HIF-1α through HREs in its promoter and a hypoxia-specific enhancer; on the other hand, *PLD2* expression is required for the full transcriptional and epigenomic rewiring promoted by hypoxia as evidenced using gene expression and chromatin accessibility analyses. In particular, the expression of stem-related genes, the opening of enhancers in the vicinity of these genes, the generation of CSCs induced by hypoxia, and the reprogramming of normal cells to iPSCs rely on normal *PLD2* expression levels. These findings indicate that PLD2 is a major player in the response to hypoxia in cancer cells that leads to increased stem cell properties resulting in higher chemoresistance.

Hypoxia is a feature of the tumor microenvironment in regions with low oxygen supply that is known to increase the stemness features of cancer cells in several types of cancer [25, 26, 51–54], including OC in which hypoxia has been shown to increase the stem-like properties of cancer cells [48]. HIF-ARNT can regulate the expression of many genes that promote the hypoxic response [6, 7]. Therefore, HIF factors may exert their effect of increasing CSCs via multiple mechanisms. In OC, HIF factors contribute to the upregulation of pluripotency factor genes, such as *SOX2* or *OCT3/4* [48, 55], proliferation pathways, such as Notch or Wnt [55, 56], or epigenetic modulation by affecting chromatin modifiers, such as SIRT1 [57]. Here we show that the OC cell lines ES-2, SKOV3 and OVCAR8 under hypoxia show upregulated expression of *PLD2*, which encodes phospholipase D2, in these cells in a Hif-1α-dependent manner (Fig. 1), as recently reported in colon cancer [45]. Using DNA binding motif analyses and reporter assays, we also demonstrate that *PLD2* expression is regulated at the transcriptional level by HREs located within the *PLD2* promoter and a hypoxia-specific enhancer that activates *PLD2* transcription in hypoxia, thus providing a mechanistic explanation of Hif-1α-mediated *PLD2* overexpression. Therefore, it is likely that the HIf-1α-PLD2 axis works in other solid tumors under hypoxic conditions.

The expression of *PLD2* is elevated in several cancer types [27, 58–63], and here, using public patient databases and our cohort of patients, we show that this is also the case in OC in which it may be related to decreased OS (Fig. 1). Furthermore, consistent with the results in OC cell lines, clustering analyses of OC patient gene expression revealed that *PLD2* expression is correlated with the rewiring of transcriptomic programs of the response to hypoxia and stem cell maintenance (Fig. 3). Indeed, we found two different clusters of patients, one of which showed gene expression patterns more different from healthy controls coinciding with higher *PLD2* expression. Although the expression of the OC marker *PAX8* and other stemness- and hypoxia-related genes was enhanced in both clusters, other markers showed increased expression only in the patient cluster with high *PLD2* expression, suggesting that PLD2 may promote stemness through specific genes or pathways as we show in *SOX2*, *SOX9* and *NOTCH1*, but not *SOX17*. These data indicate that a correlation exists between *PLD2* expression and highly altered transcriptomic programs of the response to hypoxia and stemness. In addition, we provide evidence that PLD2 is important for the alteration in the epigenomic landscape provoked by hypoxia since both hypoxia and *PLD2* overexpression in normoxia lead to similar alterations in chromatin accessibility that are counteracted by *PLD2* depletion, including the opening of enhancers in the proximity of genes related to the stem fate, which we show were upregulated (Fig. 2). These changes connect hypoxia with stemness gene expression and likely occur through the activation of CREs bound by the AP-1 family of TFs. In a previous study analysing OC tumors, solid metastasis and effusions, higher *PLD2* expression was described in effusions rather than solid tumors and metastasis [64]. This finding is consistent with our findings since OC effusions, most of which are peritoneal, are characterized by low oxygen levels and a high content in CSCs [20]. Therefore, the hypoxia-PLD2 axis seems to play a major role in the generation of ovarian CSCs.

Importantly, *PLD2* depletion partially suppresses the effect induced by hypoxia (Fig. 5), suggesting that PLD2 is an important mediator of hypoxia-induced stemness. This finding was also corroborated by reprogramming experiments of MEFs to iPSCs in which PLD2 was required for the increased reprogramming induced by hypoxia. Indeed, PLD2 might also potentiate the response to hypoxia by a positive feedback loop. This hypothesis can be supported since the combination of hypoxia and *PLD2* overexpression additively enhanced the stem properties of OC cells. The activation of HIF-1α expression or activity by PLD2 has been reported in endothelial, glioma and renal cancer cells [65–67], but there is evidence of the opposite effect in HEK293 cells [68], suggesting that this feedback loop may work in specific contexts or cell types. Nevertheless, whether the effect of PLD2 on stemness is an autocrine or a paracrine effect remains to be elucidated. In this regard, we previously showed that exosomes from *PLD2*-overexpressing colorectal cancer cells induced senescence in stromal fibroblasts [27], which, in turn, induced WNT pathway activation and increased stemness in tumor cells. In OC, hypoxia-induced

exosomes have been involved in increased tumorigenic properties and chemoresistance by several mechanisms. These include exosome-containing oncogenic proteins, such as STAT3 and FAS [69], microRNAs that altered tumor-associated macrophages [70, 71], as well as plasma gelsolin, which induces the conversion of chemosensitive OC cells to chemoresistant cells [72]. Finally, a role of PLD1 and PLD2 inducing exosome secretion in OC cells has also been recently proposed [73], suggesting that PLD2 may also influence the tumor microenvironment in OC.

Several mechanisms have been described to promote chemotherapy resistance under hypoxia in OC, including the upregulation of the *ABCG2* transporter gene, which increases drug efflux [74, 75], *c-KIT* overexpression [56] and high cysteine levels [76]. CSCs are responsible for chemotherapy resistance [21, 22], and ovarian CSCs were identified sixteen years ago and reported to be chemoresistant [77, 78]. In agreement with this idea, we previously found several markers linking ovarian CSCs and chemoresistance [28, 79]. Here, using OC cells and xenograft models, we show that the overexpression of *PLD2* leads to resistance to platinum-derived compounds, including cisplatin and carboplatin (Fig. 7). Moreover, *PLD2* expression is higher in patients resistant to platinum-based chemotherapy than in sensitive patients, confirming our results in cell lines and mouse models. This is particularly relevant in ovarian tumors, which are typically treated with platinum-based compounds and show high rates of chemoresistance, with frequent metastasis in hypoxic environments, such as abdominal ascites. How PLD2 provokes such resistance is an intriguing issue, although it is likely that its enzymatic product phosphatidic acid (PA), an important molecule acting as a second messenger in multiple cellular functions [80], might play some relevant role in avoiding chemotherapy-induced cell damage. Indeed, we previously showed that PA administration has similar effects as *PLD2* overexpression [27]. Since PA is also generated by PLD1, we cannot completely disregard a potential influence of PLD1 and PLD1-derived PA in our proposed model. However, our analysis involving the genetic depletion of *PLD2* demonstrates a significant suppression of hypoxia-induced stemness and chemoresistance and suggests that PLD2 is the primary driver of these phenotypes. However, we cannot rule out an indirect effect of PLD1, but this hypothesis would require thorough testing.

Conclusions

Our findings suggest a model in which hypoxia leads to the transcriptional overexpression of *PLD2* in OC, which, in turn, generates PA and induces the generation of chemoresistant ovarian CSCs. Therefore, we propose an alternative treatment based on a combination of cisplatin and the pharmacological inhibition of PLD2. Our in vitro and in vivo results demonstrate that this combined treatment may be useful for patients with high *PLD2* expression, who are resistant to conventional therapy with cisplatin alone.

Abbreviations

ARNT	a subunit regulated by oxygen levels and a constitutively expressed b subunit
ATAC-seq	Assay for Transposase-Accessible Chromatin using sequencing
CSCs	cancer stem cells
CREs	cis-regulatory elements
ATAC peaks	computationally called open chromatin regions
DARs	differentially accessible regions
EMT	epithelial-to-mesenchymal
GO	Gene Ontology
HIF	hypoxia-inducible factors
HREs	hypoxia-response elements
iPSC	induced pluripotent stem cell
MEFs	mouse embryonic fibroblasts
mRNA	messenger RNA
OC	Ovarian cancer
OS	overall survival
PA	phosphatidic acid
FIPI	5-Fluoro-2-indolyl des-chlorohalopemide
PPS	post-progression survival
PFS	progression-free survival
PHD2	prolyl hydroxylase 2
shRNA	small harpin RNA
siRNA	small interfering RNA
TAD	topologically associating domain
VHL	von Hippel–Lindau

Supplementary Information

The online version contains supplementary material available at https://doi.org/10.1186/s13046-024-02988-y.

Supplementary Material 1

Supplementary Material 2

Acknowledgements

The authors thank the donors and the HUVR-IBiS Biobank (Andalusian Public Health System Biobank and ISCIII-Red de Biobancos PT20/00069) for the human specimens that were used in this study.

Author contributions

SMG and AC conceived and designed this study. SMG and EMVS performed the experiments; JMSP analysed the NGS data; PEG collected the clinical data; and SMG and AC analysed and interpreted the data and drafted and edited the manuscript. All authors revised the manuscript.

Funding

This research was funded by Grants RTI2018-097455-B-I00 and PID2021-122629OB-I00 funded by MCIN/AEI and by "ERDF A way of making Europe", by the "European Union". Additional grants from CIBER de Cáncer (CB16/12/00275), from Consejeria de Salud (PI-0397-2017) and Project P18-RT-2501 from 2018 competitive research projects call within the scope of PAIDI 2020—80% co-financed by the European Regional Development Fund (ERDF) from the Regional Ministry of Economic Transformation, Industry, Knowledge and Universities. Junta de Andalucía. Special thanks to the AECC (Spanish Association of Cancer Research) Founding Ref. GC16173720CARR for supporting this work. SMG was funded by a grant from the Fundación AECC. EMV-S is funded by postdoctoral fellowships from Junta de Andalucía (DOC_01655). JMS-P is funded by an Emergia grant from Junta de Andalucía (EMC21_00188).
Open Access funding provided thanks to the CRUE-CSIC agreement with Springer Nature.

Data availability
The datasets used and/or analysed during the current study are available from the corresponding author upon reasonable request. ATAC-seq data generated in this study is available through the Gene Expression Omnibus (GEO) accession number GSE210599.

Declarations

Ethics approval and consent to participate
All methods were performed in accordance with the relevant guidelines and regulations of the Institute for Biomedical Research of Seville (IBIS) and University Hospital Virgen del Rocio (HUVR). All animal experiments and the entire procedures of the patient cohort were performed according to the experimental protocol approved by HUVR Animals Ethics (CEI 0309-N-15).

Consent for publication
Written consent for publication was obtained from all patients involved in our study.

Competing interests
The authors declare that they have no other competing financial interests.

Received: 11 December 2023 / Accepted: 15 February 2024
Published online: 26 February 2024

References

1. Harris AL. Hypoxia–a key regulatory factor in tumour growth. Nat Rev Cancer. 2002;2(1):38–47.
2. Wang GL, Semenza GL. General involvement of hypoxia-inducible factor 1 in transcriptional response to hypoxia. Proc Natl Acad Sci U S A. 1993;90(9):4304–8.
3. Ratcliffe PJ, O'Rourke JF, Maxwell PH, Pugh CW. Oxygen sensing, hypoxia-inducible factor-1 and the regulation of mammalian gene expression. J Exp Biol. 1998;201(Pt 8):1153–62.
4. Zhong H, De Marzo AM, Laughner E, Lim M, Hilton DA, Zagzag D, et al. Overexpression of hypoxia-inducible factor 1alpha in common human cancers and their metastases. Cancer Res. 1999;59(22):5830–5.
5. Wicks EE, Semenza GL. Hypoxia-inducible factors: cancer progression and clinical translation. J Clin Invest. 2022;132(11).
6. Schito L, Semenza GL. Hypoxia-inducible factors: Master regulators of Cancer Progression. Trends Cancer. 2016;2(12):758–70.
7. Kaelin WG Jr., Ratcliffe PJ. Oxygen sensing by metazoans: the central role of the HIF hydroxylase pathway. Mol Cell. 2008;30(4):393–402.
8. Jing X, Yang F, Shao C, Wei K, Xie M, Shen H, et al. Role of hypoxia in cancer therapy by regulating the tumor microenvironment. Mol Cancer. 2019;18(1):157.
9. Wilson WR, Hay MP. Targeting hypoxia in cancer therapy. Nat Rev Cancer. 2011;11(6):393–410.
10. Unruh A, Ressel A, Mohamed HG, Johnson RS, Nadrowitz R, Richter E, et al. The hypoxia-inducible factor-1 alpha is a negative factor for tumor therapy. Oncogene. 2003;22(21):3213–20.
11. Chen A, Sceneay J, Godde N, Kinwel T, Ham S, Thompson EW, et al. Intermittent hypoxia induces a metastatic phenotype in breast cancer. Oncogene. 2018;37(31):4214–25.
12. Klemba A, Bodnar L, Was H, Brodaczewska KK, Wcislo G, Szczylik CA et al. Hypoxia-mediated decrease of ovarian Cancer cells reaction to treatment: significance for chemo- and immunotherapies. Int J Mol Sci. 2020;21(24).
13. Lin SH, Koong AC. Breathing New Life into Hypoxia-targeted therapies for Non-small Cell Lung Cancer. J Natl Cancer Inst. 2018;110(1).
14. Mayer A, Hockel M, Wree A, Leo C, Horn LC, Vaupel P. Lack of hypoxic response in uterine leiomyomas despite severe tissue hypoxia. Cancer Res. 2008;68(12):4719–26.
15. Simiantonaki N, Taxeidis M, Jayasinghe C, Kurzik-Dumke U, Kirkpatrick CJ. Hypoxia-inducible factor 1 alpha expression increases during colorectal carcinogenesis and tumor progression. BMC Cancer. 2008;8:320.
16. Sun HC, Qiu ZJ, Liu J, Sun J, Jiang T, Huang KJ, et al. Expression of hypoxia-inducible factor-1 alpha and associated proteins in pancreatic ductal adenocarcinoma and their impact on prognosis. Int J Oncol. 2007;30(6):1359–67.
17. Ueda S, Saeki T, Osaki A, Yamane T, Kuji I. Bevacizumab induces Acute Hypoxia and Cancer Progression in patients with refractory breast Cancer: Multimodal Functional Imaging and Multiplex Cytokine Analysis. Clin Cancer Res. 2017;23(19):5769–78.
18. Siegel RL, Miller KD, Jemal A. Cancer statistics, 2020. CA Cancer J Clin. 2020;70(1):7–30.
19. Torre LA, Trabert B, DeSantis CE, Miller KD, Samimi G, Runowicz CD, et al. Ovarian cancer statistics, 2018. CA Cancer J Clin. 2018;68(4):284–96.
20. Munoz-Galvan S, Carnero A. Targeting Cancer Stem cells to overcome Therapy Resistance in Ovarian Cancer. Cells. 2020;9(6).
21. Batlle E, Clevers H. Cancer stem cells revisited. Nat Med. 2017;23(10):1124–34.
22. Beck B, Blanpain C. Unravelling cancer stem cell potential. Nat Rev Cancer. 2013;13(10):727–38.
23. Carnero A, Garcia-Mayea Y, Mir C, Lorente J, Rubio IT, ME LL. The cancer stem-cell signaling network and resistance to therapy. Cancer Treat Rev. 2016;49:25–36.
24. Maugeri-Sacca M, Vigneri P, De Maria R. Cancer stem cells and chemosensitivity. Clin Cancer Res. 2011;17(15):4942–7.
25. Mathieu J, Zhang Z, Zhou W, Wang AJ, Heddleston JM, Pinna CM, et al. HIF induces human embryonic stem cell markers in cancer cells. Cancer Res. 2011;71(13):4640–52.
26. Peng G, Liu Y. Hypoxia-inducible factors in cancer stem cells and inflammation. Trends Pharmacol Sci. 2015;36(6):374–83.
27. Munoz-Galvan S, Lucena-Cacace A, Perez M, Otero-Albiol D, Gomez-Cambronero J, Carnero A. Tumor cell-secreted PLD increases tumor stemness by senescence-mediated communication with microenvironment. Oncogene. 2019;38(8):1309–23.
28. Munoz-Galvan S, Felipe-Abrio B, Verdugo-Sivianes EM, Perez M, Jimenez-Garcia MP, Suarez-Martinez E, et al. Downregulation of MYPT1 increases tumor resistance in ovarian cancer by targeting the Hippo pathway and increasing the stemness. Mol Cancer. 2020;19(1):7.
29. Li H, Chen X, Calhoun-Davis T, Claypool K, Tang DG. PC3 human prostate carcinoma cell holoclones contain self-renewing tumor-initiating cells. Cancer Res. 2008;68(6):1820–5.
30. Barrandon Y, Green H. Three clonal types of keratinocyte with different capacities for multiplication. Proc Natl Acad Sci U S A. 1987;84(8):2302–6.
31. Buenrostro JD, Giresi PG, Zaba LC, Chang HY, Greenleaf WJ. Transposition of native chromatin for fast and sensitive epigenomic profiling of open chromatin, DNA-binding proteins and nucleosome position. Nat Methods. 2013;10(12):1213–8.
32. Fernandez-Minan A, Bessa J, Tena JJ, Gomez-Skarmeta JL. Assay for transposase-accessible chromatin and circularized chromosome conformation capture, two methods to explore the regulatory landscapes of genes in zebrafish. Methods Cell Biol. 2016;135:413–30.
33. Langmead B, Salzberg SL. Fast gapped-read alignment with Bowtie 2. Nat Methods. 2012;9(4):357–9.
34. Li H, Handsaker B, Wysoker A, Fennell T, Ruan J, Homer N, et al. The sequence Alignment/Map format and SAMtools. Bioinformatics. 2009;25(16):2078–9.
35. Quinlan AR, Hall IM. BEDTools: a flexible suite of utilities for comparing genomic features. Bioinformatics. 2010;26(6):841–2.
36. Haeussler M, Zweig AS, Tyner C, Speir ML, Rosenbloom KR, Raney BJ, et al. The UCSC Genome Browser database: 2019 update. Nucleic Acids Res. 2019;47(D1):D853–D8.
37. Zhang Y, Liu T, Meyer CA, Eeckhoute J, Johnson DS, Bernstein BE, et al. Model-based analysis of ChIP-Seq (MACS). Genome Biol. 2008;9(9):R137.
38. Love MI, Huber W, Anders S. Moderated estimation of Fold change and dispersion for RNA-seq data with DESeq2. Genome Biol. 2014;15(12):550.
39. Santos-Pereira JM, Gallardo-Fuentes L, Neto A, Acemel RD, Tena JJ. Pioneer and repressive functions of p63 during zebrafish embryonic ectoderm specification. Nat Commun. 2019;10(1):3049.
40. Ramirez F, Ryan DP, Gruning B, Bhardwaj V, Kilpert F, Richter AS, et al. deepTools2: a next generation web server for deep-sequencing data analysis. Nucleic Acids Res. 2016;44(W1):W160–5.
41. Grant CE, Bailey TL. XSTREME: Comprehensive motif analysis of biological sequence datasets. bioRxiv. 2021.
42. Hiller M, Agarwal S, Notwell JH, Parikh R, Guturu H, Wenger AM, et al. Computational methods to detect conserved non-genic elements in phylogenetically isolated genomes: application to zebrafish. Nucleic Acids Res. 2013;41(15):e151.
43. Bentsen M, Goymann P, Schultheis H, Klee K, Petrova A, Wiegandt R, et al. ATAC-seq footprinting unravels kinetics of transcription factor binding during zygotic genome activation. Nat Commun. 2020;11(1):4267.

44. Fornes O, Castro-Mondragon JA, Khan A, van der Lee R, Zhang X, Richmond PA, et al. JASPAR 2020: update of the open-access database of transcription factor binding profiles. Nucleic Acids Res. 2020;48(D1):D87–D92.
45. Liu M, Du K, Jiang B, Wu X. High expression of PhospholipaseD2 Induced by Hypoxia promotes proliferation of Colon cancer cells through activating NF-kappa Bp65 signaling pathway. Pathol Oncol Res. 2020;26(1):281–90.
46. Hu CJ, Sataur A, Wang L, Chen H, Simon MC. The N-terminal transactivation domain confers target gene specificity of hypoxia-inducible factors HIF-1alpha and HIF-2alpha. Mol Biol Cell. 2007;18(11):4528–42.
47. Kunz M, Ibrahim SM. Molecular responses to hypoxia in tumor cells. Mol Cancer. 2003;2:23.
48. Liang D, Ma Y, Liu J, Trope CG, Holm R, Nesland JM, et al. The hypoxic microenvironment upgrades stem-like properties of ovarian cancer cells. BMC Cancer. 2012;12:201.
49. Yoshida Y, Takahashi K, Okita K, Ichisaka T, Yamanaka S. Hypoxia enhances the generation of induced pluripotent stem cells. Cell Stem Cell. 2009;5(3):237–41.
50. Ganesan R, Mahankali M, Alter G, Gomez-Cambronero J. Two sites of action for PLD2 inhibitors: the enzyme catalytic center and an allosteric, phosphoinositide biding pocket. Biochim Biophys Acta. 2015;1851(3):261–72.
51. Li Z, Bao S, Wu Q, Wang H, Eyler C, Sathornsumetee S, et al. Hypoxia-inducible factors regulate tumorigenic capacity of glioma stem cells. Cancer Cell. 2009;15(6):501–13.
52. Schwab LP, Peacock DL, Majumdar D, Ingels JF, Jensen LC, Smith KD, et al. Hypoxia-inducible factor 1alpha promotes primary tumor growth and tumor-initiating cell activity in breast cancer. Breast Cancer Res. 2012;14(1):R6.
53. Wang Y, Liu Y, Malek SN, Zheng P, Liu Y. Targeting HIF1alpha eliminates cancer stem cells in hematological malignancies. Cell Stem Cell. 2011;8(4):399–411.
54. Carnero A, Lleonart M. The hypoxic microenvironment: a determinant of cancer stem cell evolution. BioEssays. 2016;38(Suppl 1):65–74.
55. Seo EJ, Kim DK, Jang IH, Choi EJ, Shin SH, Lee SI, et al. Hypoxia-NOTCH1-SOX2 signaling is important for maintaining cancer stem cells in ovarian cancer. Oncotarget. 2016;7(34):55624–38.
56. Chau WK, Ip CK, Mak AS, Lai HC, Wong AS. c-Kit mediates chemoresistance and tumor-initiating capacity of ovarian cancer cells through activation of Wnt/beta-catenin-ATP-binding cassette G2 signaling. Oncogene. 2013;32(22):2767–81.
57. Qin J, Liu Y, Lu Y, Liu M, Li M, Li J, et al. Hypoxia-inducible factor 1 alpha promotes cancer stem cells-like properties in human ovarian cancer cells by upregulating SIRT1 expression. Sci Rep. 2017;7(1):10592.
58. Carnero A, Cuadrado A, del Peso L, Lacal JC. Activation of type D phospholipase by serum stimulation and ras-induced transformation in NIH3T3 cells. Oncogene. 1994;9(5):1387–95.
59. Henkels KM, Boivin GP, Dudley ES, Berberich SJ, Gomez-Cambronero J. Phospholipase D (PLD) drives cell invasion, tumor growth and metastasis in a human breast cancer xenograph model. Oncogene. 2013;32(49):5551–62.
60. Saito M, Iwadate M, Higashimoto M, Ono K, Takebayashi Y, Takenoshita S. Expression of phospholipase D2 in human colorectal carcinoma. Oncol Rep. 2007;18(5):1329–34.
61. Zheng Y, Rodrik V, Toschi A, Shi M, Hui L, Shen Y, et al. Phospholipase D couples survival and migration signals in stress response of human cancer cells. J Biol Chem. 2006;281(23):15862–8.
62. Frankel P, Ramos M, Flom J, Bychenok S, Joseph T, Kerkhoff E, et al. Ral and rho-dependent activation of phospholipase D in v-Raf-transformed cells. Biochem Biophys Res Commun. 1999;255(2):502–7.
63. Song JG, Pfeffer LM, Foster DA. v-Src increases diacylglycerol levels via a type D phospholipase-mediated hydrolysis of phosphatidylcholine. Mol Cell Biol. 1991;11(10):4903–8.
64. Harel-Dassa K, Yedgar S, Trope CG, Davidson B, Reich R. Phospholipase D messenger RNA expression and clinical role in high-grade serous carcinoma. Hum Pathol. 2017;62:115–21.
65. Ghim J, Moon JS, Lee CS, Lee J, Song P, Lee A, et al. Endothelial deletion of phospholipase D2 reduces hypoxic response and pathological angiogenesis. Arterioscler Thromb Vasc Biol. 2014;34(8):1697–703.
66. Han S, Huh J, Kim W, Jeong S, Min do S, Jung Y. Phospholipase D activates HIF-1-VEGF pathway via phosphatidic acid. Exp Mol Med. 2014;46:e126.
67. Toschi A, Edelstein J, Rockwell P, Ohh M, Foster DA. HIF alpha expression in VHL-deficient renal cancer cells is dependent on phospholipase D. Oncogene. 2008;27(19):2746–53.
68. Park MH, Bae SS, Choi KY, Min do S. Phospholipase D2 promotes degradation of hypoxia-inducible factor-1alpha independent of lipase activity. Exp Mol Med. 2015;47:e196.
69. Dorayappan KDP, Wanner R, Wallbillich JJ, Saini U, Zingarelli R, Suarez AA, et al. Hypoxia-induced exosomes contribute to a more aggressive and chemoresistant ovarian cancer phenotype: a novel mechanism linking STAT3/Rab proteins. Oncogene. 2018;37(28):3806–21.
70. Chen X, Zhou J, Li X, Wang X, Lin Y, Wang X. Exosomes derived from hypoxic epithelial ovarian cancer cells deliver microRNAs to macrophages and elicit a tumor-promoted phenotype. Cancer Lett. 2018;435:80–91.
71. Zhu X, Shen H, Yin X, Yang M, Wei H, Chen Q, et al. Macrophages derived exosomes deliver miR-223 to epithelial ovarian cancer cells to elicit a chemoresistant phenotype. J Exp Clin Cancer Res. 2019;38(1):81.
72. Asare-Werehene M, Nakka K, Reunov A, Chiu CT, Lee WT, Abedini MR, et al. The exosome-mediated autocrine and paracrine actions of plasma gelsolin in ovarian cancer chemoresistance. Oncogene. 2020;39(7):1600–16.
73. Onallah H, Mannully ST, Davidson B, Reich R. Exosome Secretion and epithelial-mesenchymal transition in Ovarian Cancer are regulated by Phospholipase D. Int J Mol Sci. 2022;23(21).
74. He M, Wu H, Jiang Q, Liu Y, Han L, Yan Y, et al. Hypoxia-inducible factor-2alpha directly promotes BCRP expression and mediates the resistance of ovarian cancer stem cells to adriamycin. Mol Oncol. 2019;13(2):403–21.
75. Wang WJ, Sui H, Qi C, Li Q, Zhang J, Wu SF, et al. Ursolic acid inhibits proliferation and reverses drug resistance of ovarian cancer stem cells by down-regulating ABCG2 through suppressing the expression of hypoxia-inducible factor-1alpha in vitro. Oncol Rep. 2016;36(1):428–40.
76. Nunes SC, Ramos C, Lopes-Coelho F, Sequeira CO, Silva F, Gouveia-Fernandes S, et al. Cysteine allows ovarian cancer cells to adapt to hypoxia and to escape from carboplatin cytotoxicity. Sci Rep. 2018;8(1):9513.
77. Bapat SA, Mali AM, Koppikar CB, Kurrey NK. Stem and progenitor-like cells contribute to the aggressive behavior of human epithelial ovarian cancer. Cancer Res. 2005;65(8):3025–9.
78. Hu L, McArthur C, Jaffe RB. Ovarian cancer stem-like side-population cells are tumourigenic and chemoresistant. Br J Cancer. 2010;102(8):1276–83.
79. Munoz-Galvan S, Felipe-Abrio B, Garcia-Carrasco M, Dominguez-Pinol J, Suarez-Martinez E, Verdugo-Sivianes EM, et al. New markers for human ovarian cancer that link platinum resistance to the cancer stem cell phenotype and define new therapeutic combinations and diagnostic tools. J Exp Clin Cancer Res. 2019;38(1):234.
80. Jang JH, Lee CS, Hwang D, Ryu SH. Understanding of the roles of phospholipase D and phosphatidic acid through their binding partners. Prog Lipid Res. 2012;51(2):71–81.

Publisher's Note